Microscopic analytical theory of a correlated, two-dimensional ***N***-electron gas in a magnetic field

1997 J. Phys.: Condens. Matter 9 5889

(http://iopscience.iop.org/0953-8984/9/27/018)

J. Phys.: Condens. Matter **9** (1997) 5889–5920. Printed in the UK PII: S0953-8984(97)81318-5

Microscopic analytical theory of a correlated, two-dimensional N-electron gas in a magnetic field

Neil F Johnson†§ and Luis Quiroga‡

† Department of Physics, Oxford University, Parks Road, Oxford OX1 3PU, UK

‡ Departamento de Fisica, Universidad de Los Andes, Bogota, Apartado Aereo 4976, Colombia

Received 27 January 1997, in final form 6 May 1997

Abstract. We present a microscopic, analytical theory describing a confined N-electron gas in two dimensions subject to an external magnetic field. The number of electrons N and strength of the electron–electron interaction can be arbitrarily large, and all Landau levels are included implicitly. For any value of the magnetic field B, the correlated N-electron states are determined by the solution to a universal effective problem which resembles that of a fictitious particle moving in a multi-dimensional space, without a magnetic field, occupied by potential minima corresponding to the classical N-electron equilibrium configurations. Introducing the requirement of total wavefunction antisymmetry selects out the allowed minimum-energy N-electron states. It is shown that low-energy minima can exist at filling factors $\nu = p/(2n+1)$ where p and n are any positive integers. These filling factors correspond to the experimentally observed fractional (FQHE) and integer (IQHE) quantum Hall effects. The energy gaps calculated analytically at $\nu = p/3$ are found to be consistent with experimental data as a function of magnetic field, over a range of samples.

1. Introduction

The problem of a highly correlated, two-dimensional electron gas in an external magnetic field has attracted much attention in the past decade. Of particular interest is the microscopic origin of the observed fractions in the fractional quantum Hall effect (FQHE) [1–3]. In the past few years, it has also been appreciated that many-body effects play a role in the formation of the gaps giving rise to the integer quantum Hall effect (IQHE). As a complement to the experimental work on this subject, there have been many theoretical models proposed for both the FQHE and the IQHE. These range from field-theoretical treatments through to numerical, finite-size ($N \leqslant 6$) calculations. One of the most successful theoretical developments has been the proposal of trial wavefunctions by Laughlin and others [1, 3–5] to describe the interplay of wavefunction antisymmetry and electron–electron repulsion that effectively allows electrons in the lowest Landau level to form a highly correlated electron liquid. A related development by Jain [6] considers the construction of 'composite' fermions by attaching flux tubes to each electron—recent work on Chern–Simons field theories provides some support for such composite-fermion construction schemes [3, 7]. The general problem of describing an N-electron gas in an external magnetic field has recently taken on additional importance in semiconductor physics due to the fabrication of quantum dots containing a finite number of electrons [8–10]. It is interesting to note that although the FQHE was originally observed in infinite

§ E-mail: n.johnson@physics.oxford.ac.uk.

0953-8984/97/275889+32$19.50

two-dimensional electron gases (2DEG), it even persists in quantum dots containing a large but finite number N of electrons [11].

Given the fact that the underlying, microscopic N-electron Hamiltonian is known, one could ask whether there exists an alternative, more direct way of understanding the nature of highly correlated electron states *without* recourse to composite-fermion constructions, effective-field theories, restrictions to lowest Landau levels, and/or small numbers of electrons. The obvious stumbling blocks are that the electron–electron repulsion and the cyclotron energy are typically comparable in magnitude, and that N-electron Schrödinger equations are generally intractable analytically.

In this paper we pursue such an alternative approach, starting with an N-electron Schrödinger equation. We develop a microscopic, analytical theory describing correlated states of a confined N-electron gas in two dimensions subject to an external magnetic field B. The number of electrons N and the strength of the electron–electron interaction can be arbitrarily large, and all Landau levels are included implicitly. We show that the description of N-electron correlated states at finite B reduces to a universal effective problem which resembles that of a fictitious particle moving in a multi-dimensional space occupied by potential minima corresponding to the classical N-electron equilibrium configurations. Introducing the requirement of N-electron wavefunction antisymmetry selects out the allowed minimum-energy N-electron states. A possible connection with the FQHE and IQHE is then proposed. In particular, it is argued that low-energy minima can form at particular angular momenta corresponding to filling factors $\nu = p/(2n+1)$ where p and n are any integers. These filling factors correspond to those observed experimentally for the FQHE and IQHE.

The present theory suggests the following possible physical interpretation of FQHE and IQHE states. Consider an N-electron wavefunction localized around a Wigner crystal (WX) configuration with total relative angular momentum J. At particular values of J, N-electron wavefunctions localized around nearby defect configurations (i.e. WX plus defect which we shall denote as WXD) can coexist; we note that the allowed values of J such that N-electron states can coexist around WX and WXD simultaneously are severely restricted by the requirement of total wavefunction antisymmetry. At these common J-values, which we shall denote as $J = J_m$, hybridization of the N-electron states centred on the WX and WXD minima can occur. This hybridization effectively allows the electrons in the WX solid to diffuse throughout the system via WXD defect states. The resulting delocalized 'liquid'-like N-electron state has a lower zero-point energy—a gap therefore opens up between the liquid-like states at $J = J_m$ and other states at $J \neq J_m$. For large N, the resulting liquid-like ground-states at $J = J_m$ have filling factors given by the well-known formula [3] $\nu = N(N-1)/2J_m$. *We find that the ν-values at which these gaps arise are identical to those observed experimentally in the FQHE and IQHE*. The energy gaps calculated analytically at $\nu = p/3$ are found to be consistent with experimental data obtained from a range of samples. Various other known features of FQHE states can also be reproduced.

The model avoids discussion of one-electron properties such as Landau levels, and therefore offers the possibility of a unified description of both the FQHE and IQHE based on a microscopic N-electron Schrödinger equation. The formalism in this paper builds on an earlier model presented by us in reference [12]. In particular, we conjectured in reference [12] that the classical minimum-energy configurations play a crucial role in deciding the symmetry-allowed N-electron correlated states in few-electron quantum dots. It was pointed out that the classical minimum-energy configurations for $N < 6$ all consist of N particles on a ring, while for $N = 6$, additional minima occur [13, 14]. Curiously, it is precisely at $N = 6$ that the magic-number J-sequence of $\Delta J = N$ is broken. This idea was independently

pursued by Maksym in a fascinating way [15] for $N \leqslant 6$—the classical Eckardt frame was employed to study correlated few-electron dynamics and, in particular, the possible existence of 'liquid'-like states. We note that the term 'liquid'-like was introduced by Maksym to describe the loss of symmetry occurring when states corresponding to different classical minima are allowed to mix. This terminology will also be used in the present paper. We wish to emphasize that the model presented here is qualitatively different from an earlier theoretical approach of Kivelson *et al* [16] based on the so-called cooperative ring exchange. In short, we are suggesting here that FQHE states are the liquid-like states resulting from the hybridization of N-electron wavefunctions localized around both crystal (WX) and crystal-plus-defect configurations (WXD).

The outline of the paper is as follows. In section 2 we present the microscopic N-electron Schrödinger equation. The hyperangular coordinate system is introduced for the relative-motion Hamiltonian. The problem then reduces to a $2N-4$ hyperangular equation (section 2.1). In section 2.2 the specific case of $N=3$ is outlined. This was discussed in detail in reference [12], and is reviewed here since it is useful for visualizing the N-electron results. In section 2.3 a simplified hyperangular equation is obtained which is valid in the regime of strong electron–electron interactions and for large N. The characteristics of the lowest-energy solutions are discussed. Section 3 addresses the requirement of N-electron wavefunction antisymmetry. Permutation symmetries of the N-electron wavefunction become space-group operations in the multi-dimensional hyperangular configuration space. The states which will become ground states separated by a finite energy gap are found to correspond to filling fractions observed in the FQHE. Section 4 obtains analytic estimates for the FQHE gaps at the fractions $p/3$ as an example. These estimates are found to be consistent with experimental data over a range of samples, despite the fact that the results emerge from a simple one-dimensional, particle-in-a-box equation. Section 5 summarizes the results.

2. The microscopic N-electron Hamiltonian

The analytical tractability of our model is achieved via a combination of a parabolic confinement potential and an inverse-square electron–electron repulsion potential. The parabolic confinement is known to be a reasonable approximation for many semiconductor quantum dot samples [17]. For the case of a heterostructure (i.e. a 2DEG) it mimics the effect of a positive background, yielding an approximately uniform electron density in the large-N limit (see reference [14]). The β/r^2 electron–electron interaction ($\beta > 0$) is not unrealistic in quantum dots due to the presence of image charges in neighbouring electrodes. Recent theoretical work suggests [18] that the true repulsive interaction between electrons in a quantum dot is more likely to be proportional to $1/r^n$ with $n \sim 3$ at large r and $n \sim 1$ at small r. In heterostructures, the electron–electron interaction is probably less affected by image-charge effects. However, the general features of our results, which are based on the assumption that $n = 2$ for all r, should still be qualitatively useful. In particular, the occurrence of the FQHE in two-dimensional electron gases is not thought to depend crucially on the precise form of the electron–electron repulsion. Recent quantitative comparisons [17, 19, 20] have indeed shown that the $1/r^2$ and $1/r$ repulsive interactions yield N-electron energy spectra with very similar features. Of particular relevance to the present theory is the finding that the *classical* minimum-energy configurations for N electrons in a two-dimensional parabolic confinement potential seem to be very similar for $1/r$ and $1/r^2$ interactions [21].

The exact Schrödinger equation for N electrons with a repulsive interaction β/r^2,

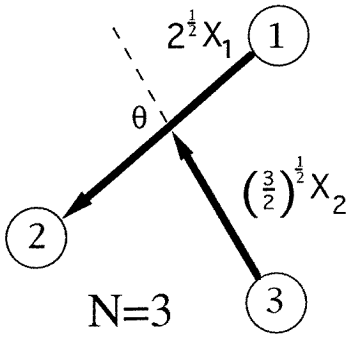

Figure 1. Jacobi coordinates for the $N = 3$ electron system. Reading clockwise, the classical configuration for three repulsive particles $\Omega_0' \equiv (132)$ corresponds to $(\alpha, \theta) = (\pi/4, \pi/2)$ (i.e. $(x, y) = (0, 0)$); the other classical configuration $\Omega_1' \equiv (123)$ corresponds to $(\alpha, \theta) = (\pi/4, -\pi/2)$ (i.e. $(x, y) = (0, \pi)$ or, equivalently, $(0, -\pi)$).

moving in a 2D parabolic potential subject to a magnetic field B (symmetric gauge) along the z-axis, is given by $(H_{\rm space} + H_{\rm spin})\Psi = E\Psi$;

$$H_{\rm space} = \sum_{i=1}^{N}\left(\frac{(\boldsymbol{p}_i - e\boldsymbol{A}_i/c)^2}{2m^*} + \frac{1}{2}m^*\omega_0^2|\boldsymbol{r}_i|^2\right) + \sum_{i<j}\frac{\beta}{|\boldsymbol{r}_i - \boldsymbol{r}_j|^2}$$
$$= \sum_{i=1}^{N}\left(\frac{\boldsymbol{p}_i^2}{2m^*} + \frac{1}{2}m^*\omega_0^2(B)|\boldsymbol{r}_i|^2 + \frac{\omega_c}{2}l_i\right) + \sum_{i<j}\frac{\beta}{|\boldsymbol{r}_i - \boldsymbol{r}_j|^2} \qquad (1)$$

where $\omega_0^2(B) = \omega_0^2 + \omega_c^2/4$, ω_c is the cyclotron frequency, and $H_{\rm spin} = -g^*\mu_B B\sum_i s_{i,z}$. The momentum and position of the ith particle are given by 2D vectors $\boldsymbol{p}_i$ and $\boldsymbol{r}_i$ respectively; l_i is the z-component of the angular momentum. The exact eigenstates are written in terms of products of spatial and spin eigenstates obtained from $H_{\rm space}$ and $H_{\rm spin}$ respectively. The eigenstates of $H_{\rm spin}$ are just products of the spinors of the individual electrons, and have energy $E_{\rm spin} = g^*\mu_B B S_z$, where S_z is the z-component of the total spin, and g^* is the electron effective g-factor. We employ standard Jacobi coordinates $\boldsymbol{X}_j$ $(j = 1, 2, \ldots, N)$ where $\boldsymbol{X}_1 = (1/N)\sum_j \boldsymbol{r}_j$ (centre-of-mass coordinate), and $\boldsymbol{X}_{j>1}$ (relative coordinates) is given by

$$\boldsymbol{X}_j = \left[\frac{j-1}{j}\right]^{1/2}\left[\boldsymbol{r}_j - \frac{1}{j-1}(\boldsymbol{r}_1 + \boldsymbol{r}_2 + \cdots + \boldsymbol{r}_{j-1})\right] \qquad (2)$$

together with the conjugate momenta $\boldsymbol{P}_j$ (see figure 1 for $N = 3$). The centre-of-mass motion decouples, $H_{\rm space} = H_{\rm CM}(\boldsymbol{X}_1) + H_{\rm rel}(\{\boldsymbol{X}_{j>1}\})$, and hence $E_{\rm space} = E_{\rm CM} + E_{\rm rel}$. The exact eigenstates of $H_{\rm CM}$ and energies $E_{\rm CM}$ are well known [23]. The non-trivial problem is that of solving the relative-motion equation $H_{\rm rel}\psi = E_{\rm rel}\psi$. We transform the relative coordinates $\{\boldsymbol{X}_{j>1}\}$ to standard hyperspherical coordinates:

$$\boldsymbol{X}_j = r\left(\prod_{i=j+1}^{N}\cos\alpha_i\right)\sin\alpha_j e^{i\theta_j}$$

with $r \geqslant 0$ and $0 \leqslant \alpha_j \leqslant \pi/2$ $(\alpha_2 = \pi/2)$. Physically, the hyperradius r is just the root mean square electron–electron separation. The exact eigenstates of $H_{\rm rel}$ have the form $\psi_{\rm rel} = R(r)F(\Omega)$ where Ω denotes the $2N-3$ hyperangular $\{\theta; \alpha\}$ variables; $R(r)$ and $F(\Omega)$

are solutions of the hyperradial and hyperangular equations respectively. The hyperradial equation is given by

$$\left[\frac{\mathrm{d}^2}{\mathrm{d}r^2}+\frac{2N-3}{r}\frac{\mathrm{d}}{\mathrm{d}r}-\frac{\gamma(\gamma+2N-4)}{r^2}-\frac{r^2}{l_0^4}+\frac{2m^*(E_{\mathrm{rel}}-\hbar J\omega_c/2)}{\hbar^2}\right]R(r)=0 \tag{3}$$

where $l_0^2=\hbar(m^*\omega_0(B))^{-1}$, and J is the total *relative* angular momentum. The parameter $\gamma>0$ and is related to the eigenvalue of the B- and ω_0-independent hyperangular equation (see section 2.1). Equation (3) can be solved exactly yielding

$$E_{\mathrm{rel}}=\hbar\omega_0(B)[2n+\gamma+N-1]+J\frac{\hbar\omega_c}{2} \tag{4}$$

where n is any positive integer or zero, and

$$R(r)=\left[\frac{r}{l_0}\right]^{\gamma}L_n^{\gamma+N-2}\left(\frac{r^2}{l_0^2}\right)\mathrm{e}^{-r^2/2l_0^2}. \tag{5}$$

Equation (4) provides an exact and infinite set of relative breathing-mode excitations $2\hbar\omega_0(B)\,\Delta n$ for any N regardless of particle statistics and/or spin states. These quantum breathing modes were first reported in reference [12], and later confirmed by Geller and Vignale [24]; the classical version of these modes for the Coulomb interaction was discussed in detail by Schweigert and Peeters [25].

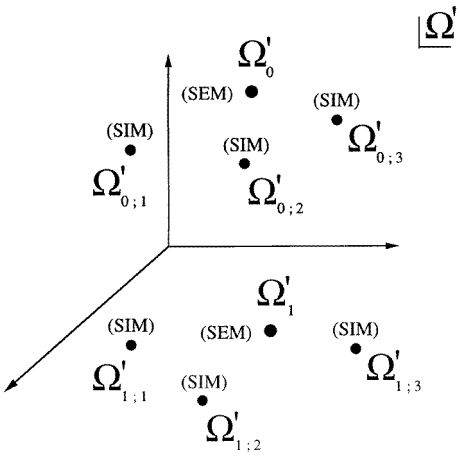

Figure 2. A schematic diagram showing a portion of the hyperangular Ω' space. Two symmetrically equivalent minima (SEMs—labelled as Ω'_i) are indicated by larger circles, while nearby symmetrically inequivalent minima (SIMs—labelled as $\Omega'_{i;a}$) are indicated by smaller circles.

2.1. The exact hyperangular equation for any N

It remains to solve the B- and ω_0-independent hyperangular equation, which is given by

$$\left[\Theta_N^2+\frac{2m^*\beta}{\hbar^2}V(\Omega)\right]F(\Omega)=[\gamma(\gamma+2N-4)]F(\Omega) \tag{6}$$

where

$$\Theta_N^2\equiv-\frac{\partial^2}{\partial\alpha_N^2}+\frac{[2N-6-(2N-4)\cos 2\alpha_N]}{\sin 2\alpha_N}\frac{\partial}{\partial\alpha_N}+\sec^2\alpha_N\Theta_{N-1}^2-\mathrm{cosec}^2\,\alpha_N\frac{\partial^2}{\partial\theta_N^2}. \tag{7}$$

The quantity $V(\Omega)$ is given by $r^2 \sum_{i<j} |\boldsymbol{r}_i - \boldsymbol{r}_j|^{-2}$, and only depends on hyperangular coordinates $\Omega \equiv \{\theta; \alpha\}$. We emphasize that this hyperangular equation (equation (6)) is universal in that it is independent of the values of the magnetic field or confinement: solving equation (6) for γ, and hence using equation (4), yields the complete solutions of the N-electron Hamiltonian H for all magnetic fields and confinement strengths. Unfortunately the hyperangular equation does not admit exact solutions for γ. Sections 2.2–2.4 will consider various approximations to equation (6) which make the problem tractable. Because J remains a good quantum number, we can introduce a Jacobi transformation of the relative-motion angles $\{\theta_i\}$: in particular,

$$\theta' = \frac{1}{N-1} \sum_{j=2}^{N} \theta_j \tag{8}$$

and

$$\theta_{[j]} = \left[\frac{j-2}{j-1}\right]^{1/2} \left[\theta_j - \frac{1}{j-2}(\theta_2 + \theta_3 + \cdots + \theta_{j-1})\right] \tag{9}$$

where $j = 3, 4, \ldots, N$. We hence have one θ'-variable, $(N-2)$ $\theta_{[j]}$-variables, $(N-2)$ α-variables, and one hyperradius r giving a total of $2N-2$ variables as required for the relative motion. The exact eigenstates of $H_{\rm rel}$ have the form $\psi = \mathrm{e}^{\mathrm{i}J\theta'} R(r) G(\Omega')$ where Ω' denotes the $(2N-4)$ $\{\theta_{[j]}; \alpha_j\}$ variables excluding θ'. The term $V(\Omega)$ is independent of θ' and will hence be written as $V(\Omega')$. It is useful to rewrite the eigenvalue of the hyperangular equation in terms of a new variable ϵ as follows:

$$\epsilon = \frac{\overline{h}^2}{8}\left[\gamma(\gamma + 2N - 4) - J^2 - \frac{2m^*\beta}{\overline{h}^2} V(\Omega'_0)\right] \tag{10}$$

where $V(\Omega'_0)$ is the value of $V(\Omega')$ evaluated at the hyperangles corresponding to a particular classical, minimum-energy N-electron configuration (a Wigner molecule). Permuting electron indices will provide a set $\{\Omega'_i\}$ of *symmetrically equivalent minima* (SEMs) [22, 15] with the same potential energy $V(\Omega'_i) \equiv V(\Omega'_0)$ for all i (e.g. Ω'_0 and Ω'_1 shown schematically in figure 2). Such SEMs have the same topological structure, but cannot be transformed into each other by rotations [22, 15]. As will be shown in section 2.2, there are two such SEMs for $N = 3$. The quantity ϵ in equation (10) accounts for the contribution to the eigenvalue of the hyperangular equation *without* including either the contributions from the rigid-body rotational energy J^2 or the electrostatic potential energy $(2m^*\beta/\overline{h}^2)V(\Omega'_0)$ of the classical minimum-energy configuration. Physically therefore, ϵ contains the zero-point energy in Ω' space associated with the quantum mechanical spread of $G(\Omega')$ about the minima $\{\Omega'_i\}$. The actual spread in $G(\Omega')$ and hence ϵ will depend on the total wavefunction antisymmetry requirement. This is illustrated for $N = 3$ in section 2.2, and discussed for large N in sections 2.3, 2.4 and 3. In general, $\epsilon \geqslant 0$, $\epsilon \sim \beta^{\mu}$ where $\mu < 1$, and $\epsilon \sim J^{\delta}$ where $\delta < 2$; these statements will be illustrated in section 2.2 for $N = 3$. It is straightforward to show that the term $(2m^*\beta/\overline{h}^2)V(\Omega'_0)$ appearing in the definition of ϵ is identical to $[V_{\rm class}/\overline{h}\omega_0(B)]^2$, where $V_{\rm class}$ is the potential energy of the classical, minimum-energy N-electron configuration, thereby recovering the expression given in reference [12]. Note that $V_{\rm class} \propto \beta^{1/2}\omega_0(B)$, and that ϵ (like γ) is independent of B and ω_0. The exact relative energy for any N can now be written as

$$E_{\rm rel} = \overline{h}\omega_0(B)\left[2n + \left([N-2]^2 + J^2 + \frac{2m^*\beta}{\overline{h}^2} V(\Omega'_0) + \frac{8\epsilon}{\overline{h}^2}\right)^{1/2} + 1\right] + J\frac{\overline{h}\omega_c}{2}. \tag{11}$$

$E_{\rm rel}$ only depends on particle statistics through ϵ. As $\overline{h} \to 0$, $\epsilon \to 0$ and $E_{\rm rel} \to V_{\rm class}$.

The exact $E_{\rm rel}$-expression has an important consequence. The J-dependence of ϵ is weaker than J^2 as $J \to 0$. Hence the term $J\hbar\omega_c/2$ in $E_{\rm rel}$ will dominate the J-dependence of $E_{\rm rel}$ for small J at fixed magnetic field ω_c. For states with $J < 0$, $E_{\rm rel}$ will hence initially decrease as $|J|$ increases. On the other hand at large negative J, $E_{\rm rel}$ will tend to $\hbar(\omega_0(B) - \omega_c/2)|J|$, and hence will increase linearly with $|J|$ at a given ω_c. This implies that $E_{\rm rel}$ has a *minimum* at a finite negative J for a given fixed magnetic field ω_c. This is the basic mechanism behind the tendency of an N-electron gas to form ground states at increasingly large J-values as the magnetic field is increased. As will be shown in section 2.2 for $N = 3$ electrons, and in section 3 for large N, only a subset of these J-minima are permitted under the requirement of total wavefunction antisymmetry. These J-values are often called 'magic-number' J-values in the context of few-electron quantum dots. In section 3 we will show that the analogous 'magic-number' J-states for a large-N electron gas constitute FQHE and IQHE states. We emphasize that so far our results are exact for any electron number N, electron–electron interaction strength β, magnetic field ω_c, and parabolic confinement ω_0.

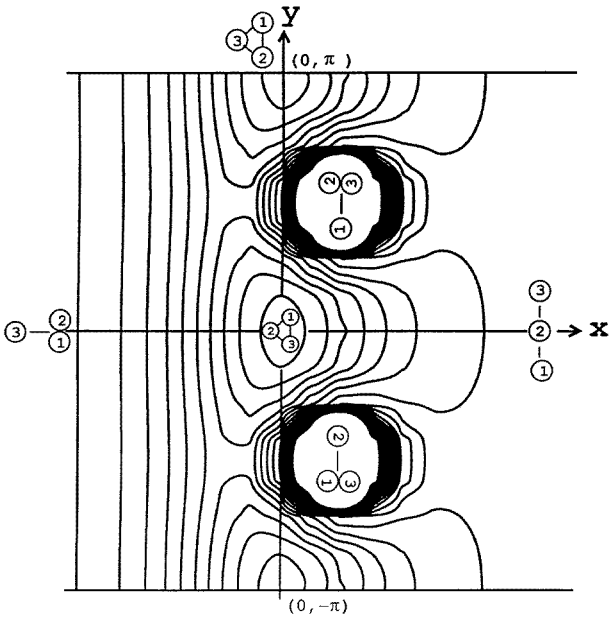

Figure 3. A contour plot of the fictitious potential $V(x, y; \epsilon)$ in the (x, y) plane for the $N = 3$ electron problem. The two symmetrically equivalent minima (SEMs—Ω_0' and Ω_1' from figure 1) are shown. Minima in $V(x, y; \epsilon)$ occur at $(0, 0)$ and $(0, \pm\pi)$ (i.e. at the classical configurations). Maxima occur at $(\ln\sqrt{3}, \pm\pi/2)$, where $V(x, y; \epsilon) \to \infty$ (i.e. electrons 2 and 3 or 1 and 3 coincident). $V(x, y; \epsilon)$ is positive and finite everywhere else. The same qualitative features appear for all ϵ ($\epsilon/m^*\beta = 5$ is used as an illustration).

2.2. The specific case of $N = 3$

This case was studied in reference [12]. Here we will summarize the results since they are important for understanding the general-N case. For convenience we change variables from α, θ (cf. figure 1) to x, y where $x = \ln[\tan(\pi/2-\alpha)]$ and $y = \theta - \pi/2$. Since $0 \leqslant \alpha \leqslant \pi/2$, then $-\infty \leqslant x \leqslant \infty$ (NB: $-\pi \leqslant y \leqslant \pi$). We define $p_x = (\hbar/\mathrm{i})\partial/\partial x$ and $p_y = (\hbar/\mathrm{i})\partial/\partial y$.

The exact hyperangular equation (equation (6)) now takes the form

$$\left[\frac{p_x^2}{2}+\frac{(p_y+\bar{h}J\cos(2\tan^{-1}\mathrm{e}^x)/2)^2}{2}+V(x,y;\epsilon)\right]G(x,y)=\epsilon G(x,y) \tag{12}$$

where

$$V(x,y;\epsilon)=m^*\beta\left[\frac{(2+\cos(2\tan^{-1}\mathrm{e}^x)}{(\mathrm{cosec}(2\tan^{-1}\mathrm{e}^x)+\cot(\tan^{-1}\mathrm{e}^x))^2-3\sin^2 y}-\frac{3}{4}\sin^2(2\tan^{-1}\mathrm{e}^x)\right.$$
$$\left.+\frac{1}{2}\cos^2(\tan^{-1}\mathrm{e}^x)+\frac{\epsilon}{m^*\beta}\cos^2(2\tan^{-1}\mathrm{e}^x)\right]. \tag{13}$$

Equation (12) represents the single-body Hamiltonian for a fictitious particle of energy ϵ and unit mass, moving in the xy-plane in a non-linear (i.e. ϵ-dependent) potential $V(x,y;\epsilon)$, subject to a fictitious, non-uniform magnetic field in the z-direction:

$$B_{\mathrm{fic}}=\frac{\bar{h}Jc}{4e}\left[1-\cos(4(\tan^{-1}\mathrm{e}^x))\right]. \tag{14}$$

B_{fic} is independent of B and has a maximum of $\bar{h}|J|c/2e$ at $x=0$ for all y. For small x, $B_{\mathrm{fic}}\approx(\bar{h}Jc/2e)(1-x^2)$. As $x\to\pm\infty$, $B_{\mathrm{fic}}\to 0$. Note we have here chosen to highlight the Schrödinger-like form of equation (12); a simple rearrangement of equation (12) shows it to be hermitian with a weighting function $\sin^2(2\tan^{-1}\mathrm{e}^x)$. These results are exact so far. Figure 3 shows the potential $V(x,y;\epsilon)$ in the (x,y) plane. $V(x,y;\epsilon)\geqslant 0$ everywhere. Minima occur at $(0,0)$ and $(0,\pm\pi)$ where $V(x,y;\epsilon)=0$ (NB $(0,\pi)$ is equivalent to $(0,-\pi)$). Maxima occur at $(\ln\sqrt{3},\pm\pi/2)$ in figure 3, where $V(x,y;\epsilon)\to\infty$. Since $\epsilon\geqslant 0$, these statements hold for any ϵ. We now discuss the physical significance of these features. The classical configurations of minimum energy (the Wigner molecule) correspond to the particles lying on a ring in the form of an equilateral triangle with $V_{\mathrm{class}}=\omega_0(B)[6m^*\beta]^{1/2}$. There are two distinct configurations, i.e. two distinct symmetrically equivalent minima [22], with clockwise orderings $\Omega_0'\equiv(132)$ and $\Omega_1'\equiv(123)$ corresponding to $(\alpha,\theta)=(\pi/4,\pm\pi/2)$. In (x,y) coordinates, these correspond to $(0,0)$ and $(0,\pi)$ (equivalently, $(0,-\pi)$). Hence the classical configurations coincide with the minima in $V(x,y;\epsilon)$ in figure 3 and the maximum in B_{fic}. As pointed out in reference [12], the formation of a Wigner molecule should therefore be favoured by both large B_{fic} (i.e. large $|J|$) and deep $V(x,y;\epsilon)$ minima (i.e. large-β, strong electron–electron interactions).

Consider the limit of very strong electron–electron interactions (i.e. $\beta\to\infty$). Since the height of the tunnel barrier between the two $V(x,y;\epsilon)$ minima is $\sim\beta$, the fictitious particle sits at one of these minima and the system is locked in one of the two classical configurations, e.g. $\Omega_0'\equiv(132)$ at $(0,0)$. The probability of tunnelling between the minima Ω_0' and Ω_1' is zero. Tunnelling between the two minima implies a mixture of configuration (123) into (132), and hence interchange of the original electrons; in many-body language, exchange effects arising from wavefunction antisymmetry are therefore negligible. ϵ is small compared to $m^*\beta$, and equation (12) reduces to

$$E_{\mathrm{rel}}=\bar{h}\omega_0(B)\left[2n+\left(1+J^2+\frac{6m^*\beta}{\bar{h}^2}\right)^{1/2}+1\right]+J\frac{\bar{h}\omega_c}{2}. \tag{15}$$

The energy $E_{\mathrm{rel}}\geqslant V_{\mathrm{class}}$, since it includes the hyperradial zero-point energy (NB $\bar{h}\to 0$ yields $E_{\mathrm{rel}}\to V_{\mathrm{class}}$ and $B_{\mathrm{fic}}\to 0$).

Next consider large but finite β. The fictitious particle now moves in the vicinity of the minimum Ω_0' (i.e. $(x,y)\approx(0,0)$). The electrons in the Wigner solid are effectively

vibrating around their classical positions. On expanding the potential $V(x, y; \epsilon)$ about $(0, 0)$ to third order, the exact equation (12) becomes

$$\left[\frac{p_x^2}{2} + \frac{(p_y - \bar{h}Jx/2)^2}{2} + \frac{1}{2}\omega_x^2 x^2 + \frac{1}{2}\omega_y^2 y^2\right] G(x, y) = \epsilon G(x, y) \tag{16}$$

where $\omega_x^2 = 3m^*\beta/4 + 2\epsilon$ and $\omega_y^2 = 3m^*\beta/4$. This has the form of a single electron moving in an anisotropic parabolic potential, subject to a uniform magnetic field $B_{\text{fic}} = \bar{h}Jc/2e$. Equation (16) is exactly solvable for ϵ using a symmetric gauge [19] (the energies are independent of the choice of gauge for B_{fic}). As an illustration, we consider small ϵ, and hence $\omega_x \approx \omega_y$. The relative energy is then given by

$$E_{\text{rel}} = \bar{h}\omega_0(B)\left(2n + \left[1 + J^2 + \frac{6m^*\beta}{\bar{h}^2} + 2(2n' + |l|' + 1) \times \left(J^2 + \frac{12m^*\beta}{\bar{h}^2}\right)^{1/2} + 2l'J\right]^{1/2} + 1\right) + J\frac{\bar{h}\omega_c}{2}. \tag{17}$$

The fictitious particle has its own set of Fock–Darwin (and hence Landau) levels [23] labelled by n' and a fictitious angular momentum l'. For large β and small n', l', and J, equation (17) yields an oscillator excitation spectrum with two characteristic frequencies $\sqrt{2}\bar{h}\omega_0(B)$ and $2\bar{h}\omega_0(B)$ representing shear and breathing modes of the Wigner molecule.

For smaller β (i.e. weaker interactions) and/or larger ϵ (i.e. excited states), the tunnelling probability between the $V(x, y; \epsilon)$ minima Ω_0' and Ω_1' in figure 3 becomes significant. The Wigner molecule begins to melt, and wavefunction antisymmetry must be included. This is discussed further in section 3. As mentioned in reference [12], the resulting analytically obtained magic-number J-transitions are found to be in good agreement with the numerical results for $1/r$ interaction. We note that the analytic results become more accurate in the Wigner solid regime (e.g. large β or $|J|$), while the numerical calculations become more computationally demanding.

2.3. Simplified hyperangular equations for arbitrarily large N

For general N, the hyperangular equation (equation (6)) is $(2N-4)$-dimensional. However, in the Wigner solid regime (large β or $|J|$), the classical minimum-energy configurations will still be important in determining ϵ and hence E_{rel}, just as for $N = 3$. Here we will consider the limit in which the number of electrons is large ($N \gg 1$). This is the limit of interest in the FQHE and in large quantum dots. Specifically, we will introduce in this section a series of approximations in order to simplify the exact hyperangular equation. At each stage, the corresponding simplified hyperangular equation is explicitly given. The resulting discussion is detailed—however, we feel that this is necessary in order to justify the successively simpler (and more approximate) hyperangular equations. Each of these simplified hyperangular equations can be solved numerically; the complexity of the algorithms needed obviously decreases as more approximations are introduced. However, the goal in this paper is to obtain a simplified version of the hyperangular equation which can be treated analytically, but which is still based on a set of reasonable approximations.

Figure 4 shows the classical ground-state configuration for $N = 230$ electrons (black dots) in a parabolic quantum dot, as obtained by Bedanov and Peeters using a Monte Carlo algorithm [14]. The rings are drawn as a guide to the eye. The number N of electrons is relatively small in the context of the $N \to \infty$ limit, and hence the details of the ground-state configuration, particularly for larger rings, will be prone to edge effects. However, the inner rings show a nearly hexagonal lattice as expected for the $N \to \infty$ limit. For the purposes

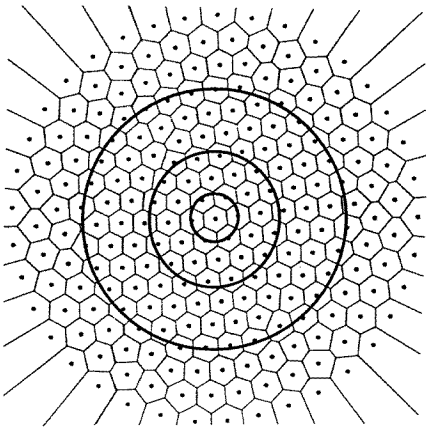

Figure 4. The ground-state classical configuration for 230 electrons (black dots) calculated numerically using a Monte Carlo simulation. This figure was adapted from figure 2 of Bedanov and Peeters (reference [14]). Straight lines are drawn to bisect the midpoint between nearest-neighbour electrons, thereby highlighting the approximately hexagonal local symmetry. Circles are drawn to illustrate the approximately ring-like arrangement of electrons. The inner circles only pass through regular hexagons. The outer circle passes through several pentagons and distorted hexagons because of its proximity to the edge of the finite cluster.

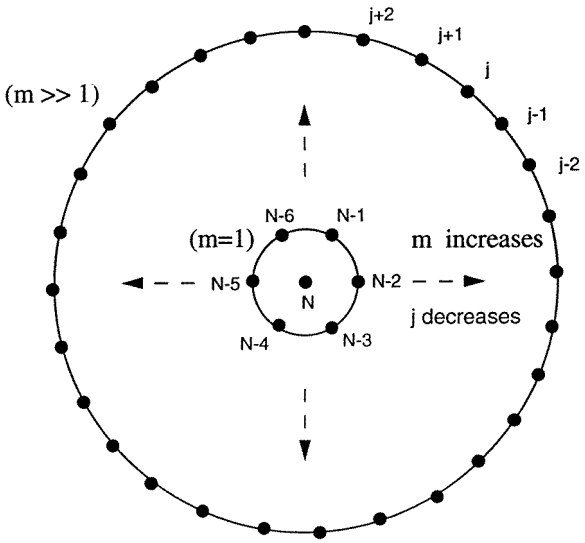

Figure 5. A particular symmetrically equivalent minimum (SEM—labelled in the text as Ω_0') with N near the centre (cf. figure 4). We are considering the limit of large N. Ring m is such that $N \gg j \gg 1$, and it is therefore far away from the circumference of the cluster.

of illustration we will therefore consider figure 4 as being representative of the $N \to \infty$ classical configuration. Consider the *particular* classical configuration Ω_0' where the Nth electron is near the centre and the first electron is on the circumference of the droplet. This is shown schematically in figure 5. As discussed in section 2.2 for $N = 3$, the fully quantum mechanical system will also lie near this configuration in Ω' space in the limit of very large

β. The jth Jacobi coordinate is given by

$$\boldsymbol{X}_j = \left[\frac{j-1}{j}\right]^{1/2} (\boldsymbol{r}_j - \boldsymbol{R}_{j-1}) \tag{18}$$

where

$$\boldsymbol{R}_{j-1} = \frac{1}{j-1}(\boldsymbol{r}_1 + \boldsymbol{r}_2 + \cdots + \boldsymbol{r}_{j-1})$$

(this quantity $\boldsymbol{R}_{j-1}$ can be thought of as the 'centre of mass' of the electrons $1, 2, \ldots, j-1$). For $j \gg 1$, and for configurations like those in figures 4 and 5 where the electrons are evenly distributed around the origin, the quantity $\boldsymbol{R}_{j-1}$ will be small compared to the typical electron lattice spacing. In addition, the prefactor $[(j-1)/j]^{1/2} \to 1$ for large j. Hence $\boldsymbol{X}_j \to \boldsymbol{r}_j$ for large j. However, there is an exact identity for hyperangular Jacobi coordinates: $\sum_{j=2}^{N}[X_j/r]^2 = 1$. Given that $X_j \to 0$ as $j \to N$ for large N, this implies that each term $[X_j/r]^2 \ll 1$ for large j. Given the definition of the hyperangular coordinates stated earlier on, it follows that the hyperangles $\alpha_j \ll 1$ for $j \gg 1$. Hence to first order in α_j, we can make the approximation $X_N = r\sin\alpha_N \approx r\alpha_N$. Similarly $X_{N-1} = r\cos\alpha_N \sin\alpha_{N-1} \approx r\alpha_{N-1}$, and, more generally, $X_j \approx r\alpha_j$. To summarize, for configurations similar to that shown in figure 5, we have the approximate result $\boldsymbol{X}_j \approx r\alpha_j e^{i\theta_j}$ in the $N \gg 1$ and $j \gg 1$ limit. There are two points to note: although we need both $j \gg 1$ and $N \gg 1$, j can still be an order of magnitude less than N. Second, the error introduced by assuming $\sin\alpha_j \approx \alpha_j$ is still reasonably small even for $j = 2$ (recall that $\alpha_2 = \pi/2 \approx 1.57$, as compared to $\sin\alpha_2 = 1$. To remain consistent within our approximation, we will take $\alpha_2 = 1$ instead of $\pi/2$ in what follows).

This approximate form for $\boldsymbol{X}_j$ leads to an interesting simplification of the exact hyperangular equation. The small-angle (i.e. $\alpha_j \ll 1$) limit of equation (6) yields

$$\left[\sum_{j=2}^{N} -\frac{\hbar^2}{2m^*}\nabla_j^2 + \beta V(\Omega)\right] F(\Omega) = \frac{\hbar^2}{2m^*}\gamma(\gamma + 2N - 4)F(\Omega) \tag{19}$$

where

$$\nabla_j^2 \equiv -\frac{\partial^2}{\partial\alpha_j^2} - \frac{1}{\alpha_j}\frac{\partial}{\partial\alpha_j} - \frac{1}{\alpha_j^2}\frac{\partial^2}{\partial\theta_j^2} \tag{20}$$

is the two-dimensional Laplacian for a fictitious particle with position (α_j, θ_j) in polar coordinates, the potential energy term

$$V(\Omega) \equiv V(\Omega') \sim \sum_{j<j'} |\alpha_j e^{i\theta_j} - \alpha_{j'} e^{i\theta_{j'}}|^{-2} \tag{21}$$

and $F(\Omega) = e^{iJ\theta'}G(\Omega')$. This equation is a good approximation for $j \to N$ with $N \gg 1$, but becomes worse as $j \to 0$ and/or $N \to 0$. (Recall that $\alpha_2 = 1$, and hence the sum can start from $j = 2$ as shown.) However, this is sufficient for the purposes of this paper, since we are interested in states that evolve within the bulk of the N-electron droplet as opposed to those at the edge. Physically, equation (19) describes a set of $N-1$ fictitious particles moving on a two-dimensional plane subject to a two-body inverse-square interaction, in the *absence* of a magnetic field. It is interesting to note that this transformation of having replaced an N-particle problem in a magnetic field with an $(N-1)$-particle problem without a magnetic field seems reminiscent of composite-fermion constructions at half-integer filling fractions. The effective Schrödinger equation in equation (19) carries the following constraint: the exact hyperangular identity $\sum_{j=2}^{N}[X_j/r]^2 = 1$ implies that $\sum \alpha_j^2 \sim 1$. This may complicate

any attempt at a solution using a 'renormalization' type of approach, such as the setting up of a recursion equation relating γ for N particles to γ for $N-1$ particles.

It is more useful to view equation (19) in the context of a single fictitious particle moving in a multi-dimensional space containing potential minima corresponding to the various classical minimum-energy configurations $\{\Omega_i'\}$. This directly connects the N-electron problem to the $N = 3$ problem discussed in section 2.2. As discussed in section 2.1, a Jacobi transformation can be undertaken on the $\{\theta_j\}$ variables. In particular,

$$\theta_{[j]} = \left[\frac{j-2}{j-1}\right]^{1/2} (\theta_j - \Theta_{j-1}) \tag{22}$$

where $j = 3, 4, \ldots, N$ and

$$\Theta_{j-1} = \frac{1}{j-2}(\theta_2 + \theta_3 + \cdots + \theta_{j-1}).$$

The quantity Θ_{j-1} represents the average of the angles θ_j, where $j = 2, 3, \ldots, j-1$. For $j \gg 1$, the quantity Θ_{j-1} will be approximately a constant, $\bar{\Theta}$, since the $j-1$ particles are evenly distributed about the origin in a given Ω_i' configuration (recall figures 4 and 5). In addition, the prefactor $[(j-2)/(j-1)]^{1/2} \to 1$ for large j. Hence $\theta_{[j]} \to \theta_j - \bar{\Theta}$ for large j, neglecting terms of order $(1/N)$. With $F(\Omega) = \mathrm{e}^{\mathrm{i}J\theta'} G(\Omega')$, equation (19) further reduces to

$$\left[\sum_{j=3}^{N} -\frac{\hbar^2}{2m^*}\left(\frac{\partial^2}{\partial\alpha_j^2} + \frac{1}{\alpha_j}\frac{\partial}{\partial\alpha_j} + \frac{1}{\alpha_j^2}\left[\frac{\partial}{\partial\theta_{[j]}} + \frac{\mathrm{i}J}{N-1}\right]^2\right) + \beta V(\Omega')\right] G(\Omega')$$
$$= \frac{\hbar^2}{2m^*}\gamma(\gamma + 2N - 4)G(\Omega'). \tag{23}$$

Again this equation is a good approximation for $j \to N$, but becomes worse as $j \to 0$. The $\{\theta_{[j]}; \alpha_j\}$ manifold carries the following constraints: $\sum \alpha_j^2 \sim 1$ and $\sum \partial/\partial\theta_{[j]} \sim 0$. The latter condition is an approximate identity for large N, and is obtained by combining

$$\sum \frac{\partial}{\partial\theta_j} = \frac{\partial}{\partial\theta'}$$

(this is an exact property of any Jacobi transformation) and

$$\frac{\partial}{\partial\theta_j} \sim \frac{\partial}{\partial\theta_{[j]}} + \frac{1}{N-1}\frac{\partial}{\partial\theta'}.$$

This new condition hence reflects the fact that the total relative angular momentum is only associated with the θ'-variable; there is no additional contribution to the relative angular momentum contained within the Ω' dynamics. These approximate constraints allow us to make a further simplification of the hyperangular equation as follows. Using the approximate identity $\sum \alpha_j^2 \sim 1$, we can define an average hyperangle $\bar{\alpha} \sim N^{-1/2}$. We will therefore replace the term

$$\sum \frac{1}{\alpha_j^2}\frac{J^2}{(N-1)^2}$$

in equation (23) by

$$\frac{1}{\bar{\alpha}^2}\sum \frac{J^2}{(N-1)^2} \sim J^2$$

assuming large N. We can hence rewrite equation (23) in the form

$$\left[\sum_{j=3}^{N} -\frac{\hbar^2}{2m^*}\left(\frac{\partial^2}{\partial\alpha_j^2}+\frac{1}{\alpha_j}\frac{\partial}{\partial\alpha_j}+\frac{1}{\alpha_j^2}\left[\frac{\partial^2}{\partial\theta_{[j]}^2}+\frac{2\mathrm{i}J}{N-1}\frac{\partial}{\partial\theta_{[j]}}\right]\right)+\beta[V(\Omega')-V(\Omega_0')]\right]G(\Omega')$$
$$=\frac{\hbar^2}{2m^*}\left[\gamma(\gamma+2N-4)-J^2-\frac{2m^*\beta}{\hbar^2}V(\Omega_0')\right]G(\Omega'). \tag{24}$$

Although its derivation has involved approximations, equation (24) merits some discussion since it elucidates several of the statements made in section 2.1. The right-hand side is just $(4/m^*)\epsilon$. Given that $\sum\alpha_j^2\sim 1$ and $\sum\partial/\partial\theta_{[j]}\sim 0$, the J-dependence of ϵ will tend to be weaker than J^2 as claimed earlier. Note that since $\sum\alpha_j^2\sim 1$, the moment of inertia I of a given classical configuration in Ω space, treated as a rigid body, is just m^*. Hence the classical rigid-body rotational energy $\hbar^2J^2/2I\sim\hbar^2J^2/2m^*$, which is precisely the term appearing in the right-hand side of equation (24). This then justifies the statement made in section 2.1 that ϵ excludes the classical rigid-body rotational energy. The term $V(\Omega_0')$ denotes $V(\Omega')$ evaluated at a given classical SEM equilibrium configuration $\Omega'\equiv\Omega_0'$. We emphasize that $V(\Omega_0')\equiv V(\Omega_i')$, i.e. the potential energy is the same for all SEMs. Since Ω_0' is a minimum, the difference term $[V(\Omega')-V(\Omega_0')]$ can be expanded around Ω_0'. The leading terms will be quadratic in $\theta_{[j]}-\theta_{[j0]}$ etc. Hence ϵ does indeed describe the zero-point energy associated with the spread in $G(\Omega')$ around the classical minima, as claimed in section 2.1 and shown explicitly for $N=3$ in section 2.2. This point is further discussed below for large N.

The hyperangular equation, equation (24), is now simpler; however, it is still not quite in a form which makes it amenable to analytic calculation. This final step can be achieved via the following considerations. Given the two approximate constraints $\sum\alpha_j^2\sim 1$ and $\sum\partial/\partial\theta_{[j]}\sim 0$, the term involving $\sum(1/\alpha_j^2)\partial/\partial\theta_{[j]}$ should be small as compared to the term involving $(1/\alpha_j^2)\partial^2/\partial\theta_{[j]}^2$, and hence will be neglected. Furthermore, just as for $N=3$, we are initially considering the quantum mechanical solution near a given classical minimum Ω_0', i.e. $\beta\to\infty$. Hence the term $(1/\alpha_j^2)\partial^2/\partial\theta_{[j]}^2$ can be approximated by $(1/\alpha_{j0}^2)\partial^2/\partial\theta_{[j]}^2$, where α_{j0} is the value of α_j at $\Omega'\equiv\Omega_0'$. The fact that Ω_0' is a minimum suggests that the leading-order expansion of $[V(\Omega')-V(\Omega_0')]$ will involve terms like $(\theta_{[j]}-\theta_{[j0]})^2$ and $(\alpha_j-\alpha_{j0})^2$ for all j, but not cross terms; this was demonstrated explicitly for $N=3$ earlier, where $V(x,y)$ was found to be a function of x^2 and y^2 but not xy. This implies the following simplification for $\Omega'\sim\Omega_0'$: $[V(\Omega')-V(\Omega_0')]\sim\sum_j[v(\alpha_j-\alpha_{j0})+w(\theta_{[j]}-\theta_{[j0]})]$ where both v and w have a minimum at $\Omega'\equiv\Omega_0'$, i.e. at $\alpha_j=\alpha_{j0}$ and $\theta_{[j]}=\theta_{[j0]}$. The approximate separability of the potential suggests that the hyperangular function $G(\Omega')$ can now be written as $f(\{\alpha_j-\alpha_{j0}\})g(\{\theta_{[j]}-\theta_{[j0]}\})$ where the functions f and g are peaked around $\Omega'\equiv\Omega_0'$. This was shown to be true explicitly for $N=3$, where f and g turned out to be gaussians (harmonic oscillator wavefunctions). Since Ω_0' is still a minimum point for large N, f and g will retain their gaussian-like character for general N. We will therefore write

$$g(\{\theta_{[j]}-\theta_{[j0]}\})\sim\prod_j g_j(\theta_{[j]}-\theta_{[j0]})$$

where $g_j(\theta_{[j]}-\theta_{[j0]})$ is a function peaked around the minimum coordinate $\theta_{[j]}=\theta_{[j0]}$. The hyperangular equation is now fully separable into an equation involving $\{\alpha_j\}$:

$$\left[\sum_{j=3}^{N} -\frac{\hbar^2}{2m^*}\left(\frac{\partial^2}{\partial\alpha_j^2}+\frac{1}{\alpha_j}\frac{\partial}{\partial\alpha_j}\right)+\beta v_j(\alpha_j-\alpha_{j0})\right]f(\{\alpha_j-\alpha_{j0}\})=E_\alpha f(\{\alpha_j-\alpha_{j0}\}) \tag{25}$$

together with the following equations for each $\theta_{[j]}$:

$$\left[-\frac{\hbar^2}{2m^*\alpha_{j0}^2}\frac{\partial^2}{\partial\theta_{[j]}^2} + \beta w_j(\theta_{[j]} - \theta_{[j0]}) \right] g_j(\theta_{[j]} - \theta_{[j0]}) = e_j g_j(\theta_{[j]} - \theta_{[j0]}). \tag{26}$$

The relation between ϵ, E_α, and e_j is as follows: $(4/m^*)\epsilon = E_\theta + E_\alpha$ where $E_\theta = \sum_j e_j$. The full expression for the relative energy hence becomes

$$E_{\rm rel} = \hbar\omega_0(B)\left[2n + \left([N-2]^2 + J^2 + \frac{2m^*\beta}{\hbar^2}V(\Omega_0') + \frac{2m^*}{\hbar^2}[E_\theta + E_\alpha] \right)^{1/2} + 1 \right] + J\frac{\hbar\omega_c}{2}. \tag{27}$$

Since equations (25) and (26) have a Schrödinger-like form with E_α and e_j as eigenvalues respectively, we will refer to these two quantities as 'energies' even though this is not strictly correct terminology.

2.4. Characteristics of the low-energy solutions $G(\Omega')$

So far we have considered the solutions near a particular minimum configuration Ω_0', i.e. we have considered very large β just as we did initially for $N = 3$. Very large β implies that $G(\Omega')$ will be peaked around one of the SEMs, e.g. around Ω_0'. In the limit of zero tunnelling between SEMs, the solution $G(\Omega') \sim f(\{\alpha_j - \alpha_{j0}\})g(\{\theta_{[j]} - \theta_{[j0]}\})$ centred at Ω_0' will be *degenerate* with the identically localized solutions centred at all other SEMs $\{\Omega_i'\}$. These localized functions can be thought of as atomic-like orbitals in Ω' space. In particular there will be a set of orbitals associated with each SEM Ω_i'. The corresponding coordinates and hyperangular equations describing these solutions are identical to those obtained earlier in section 2.3; however, the spatial ordering of the electrons for the various Ω_i' minima will necessarily change; for example, electron N will not necessarily be close to the centre. Using the usual variational argument for Schrödinger-like equations, the lowest-energy (i.e. lowest-E_α and lowest-E_θ) solutions of equations (26) and (27) will be those with the minimum number of nodes.

For large but finite β, there will be a small but finite tunnelling between the various minima $\{\Omega_i'\}$, and hence the complete solution $G(\Omega')$ will be more correctly described as a linear combination of the atomic-like solutions, just like in a single-particle tight-binding model. Furthermore, for $N \geqslant 6$, as noted earlier, there will be additional classical minima which are not topologically equivalent; again borrowing from the language of molecular physics [15, 22] these minima are termed *symmetrically inequivalent minima* (SIMs). These SIMs are local minima in Ω' space which are often just slightly higher in energy than the SEMs $\{\Omega_i\}$. In the large-N limit, these minima correspond to defect states in a hexagonal crystal. Fisher, Halperin and Morf [26] showed that a Wigner crystal with a localized defect (WXD) can be quite close in energy to the perfect Wigner crystal (WX). This finding was recently verified in the context of N electrons in a two-dimensional parabolic quantum dot by Bolton and Rossler [13] and Bedanov and Peeters [14]. These authors all found that the global minimum for the classical N-electron system tends towards a hexagonal crystal as $N \to \infty$, as expected for the Wigner crystal (WX). However, configurations corresponding to a Wigner crystal with single defects (WXD) are only slightly higher in energy. In the language of the present paper, the WX represents the SEMs while the WXD represents the SIMs. Although the SIMs are not true global minima, the complete solution $G(\Omega')$ should certainly include finite mixing with them. This is particularly true since the 'nearest neighbours' of a given SEM in Ω' space are SIMs. This is simply a consequence of the fact that translation between two adjacent SEMs in Ω' space requires interchange

of at least two electrons, while translation between a given SEM and its nearest SIMs requires only slight electron distortion. Each SEM minimum Ω_i will have p defect states as its nearest neighbours in Ω' space—we denote these nearby SIM minima as $\{\Omega'_{i;a}\}$ where $a = 1, 2, \ldots, p$ (cf. figure 2).

The resulting wavefunction $G(\Omega')$ will therefore resemble a tight-binding LCMO (linear combination of molecular orbitals) wavefunction, where each 'molecule' consists of 'atomic' orbitals on one of the SEM minima Ω_i mixed with 'atomic' orbitals on each of its nearby SIM minima. We emphasize that $N = 3$ has no SIM minima. $N = 6$ is the smallest N having SIMs. The SIMs for $N = 6$ consist of a six-member ring configuration while the SEMs contain a five-member ring plus one electron at the centre [13, 14]. For general N, the low-energy solutions should therefore be reasonably well described by

$$G(\Omega') \sim \sum_{i}^{SEM} \sum_{a}^{SIM} c_{i;a} f(\{\alpha_j - \alpha_{ji;a}\}) g(\{\theta_{[j]} - \theta_{[ji;a]}\}). \tag{28}$$

It is well known from elementary tight-binding theory that the lowest-energy states are 'bonding' wavefunctions of s orbitals. In the present context, we similarly expect the lowest energy $G(\Omega')$ to have as few nodes as possible (i.e. it will be gaussian-like around each of the SEM $\{\Omega'_i\}$, thereby resembling an s orbital); it will also correspond to the coefficients $c_{i;a}$ being identical for each i (i.e. it will resemble a 'bonding' state).

3. Fermion statistics, magic numbers, and filling fractions

So far we have not introduced the requirement that the total N-electron wavefunction be antisymmetric. In this section, we will show that it is precisely this requirement that produces the observed FQHE filling factors for large N.

It is useful to first discuss the effect of antisymmetry in the case of $N = 3$ electrons before considering large N. For three spin-polarized electrons, ψ must be antisymmetric under particle interchange $i \leftrightarrow j$. The hyperradial part $R(r)$ is invariant; particle permutation operations in $(\boldsymbol{r}_1, \boldsymbol{r}_2, \boldsymbol{r}_3)$ become straightforward *space-group* operations in the (x, y) plane. For small (x, y), $1 \leftrightarrow 2$ is equivalent to $(x, y) \rightarrow (x, y + \pi)$ with $\theta' \rightarrow \theta' + \pi/2$; $1 \leftrightarrow 3$ is equivalent to $(x, y) \rightarrow (\bar{x}, \bar{y} - \pi)$ with $\theta' \rightarrow \theta' + \pi/6$ $((\bar{x}, \bar{y})$ represents (x, y) rotated by $4\pi/3)$; $2 \leftrightarrow 3$ is equivalent to $(x, y) \rightarrow (\tilde{x}, \tilde{y} + \pi)$ with $\theta' \rightarrow \theta' - \pi/6$ $((\tilde{x}, \tilde{y})$ represents (x, y) rotated by $-4\pi/3)$. The solutions $G(x, y)$ of equation (12) with the lowest possible ϵ, and hence the lowest E_{rel} at a given ω_c, should be nodeless in the vicinity of $(0, 0)$ (cf. the ground state in the parabolic potential with $n' = 0 = l'$ in equation (17)). However, the above symmetry requirements forbid such a nodeless solution unless $e^{i\pi 2J/3} = 1$. Therefore the only symmetry-allowed solutions $G(x, y)$ which are nodeless are those where J is a multiple of three, as observed in numerical calculations for $N = 3$ electrons with a $1/r$ interaction. It is important to note that this condition, i.e. $e^{i\pi 2J/3} = 1$, just arises from combining the effect of any two sets of particle interchanges $i \leftrightarrow j$. For $N = 3$, two sets of particle interchanges correspond to rotations of a given SEM; this can be seen simply as follows. Consider a given SEM in figure 3, e.g. $\Omega'_0 \equiv (132)$. Interchanging $1 \leftrightarrow 2$ and $2 \leftrightarrow 3$ yields the *same* SEM, i.e. (132), rotated anticlockwise by $2\pi/3$. Hence combinations of two sets of particle interchanges merely rotate the Wigner molecule without involving a transformation from one SEM to another, i.e. without moving from (132) to (123). Hence in order to obtain the 'magic' angular momentum values for $N = 3$, it is *sufficient* to consider the subset of particle interchanges from the S_3 permutation group which correspond to point-group

rotations C_3, i.e. those which do not correspond to translations between SEMs. This result is discussed by Maksym in reference [15] following earlier work on molecules by Wilson [22]. Maksym also argued that for $N = 3$ the remaining permutations which correspond to translations between SEMs, and hence the effect of tunnelling between SEMs, represents a small perturbation which does not affect the magic J-values. In contrast, for $N = 6$, where topologically distinct classical configurations coexist, the tunnelling between SEMs and SIMs plays a crucial role in determining the J-values of the low-energy ground states of the system. In particular, Maksym pointed out that tunnelling between SEMs and SIMs should be most favourable when the SEM and SIM configurations have a common J-value. This is consistent with analogous ideas in single-particle tight-binding theory, where the overlap matrix element (and hence the bandwidth) is larger between s orbitals than between s and p orbitals. Maksym conjectured that the resulting tunnelling might lead to 'liquid'-like states with a lower overall energy.

These considerations motivate us to follow a similar strategy for N electrons. In particular, we will show that considering just a subset of particle interchanges of S_N corresponding to rotations of rings within the Wigner molecule (WX) and Wigner molecule plus defect (WXD) is *sufficient* to determine the magic J-values corresponding to the observed FQHE filling factors. As for $N = 3$, we focus on the vicinity of a given SEM, e.g. Ω_0'. Following the discussion in section 2.3, interchanging $\boldsymbol{r}_i \leftrightarrow \boldsymbol{r}_j$ is relatively straightforward for $i, j \gg 1$ since $\boldsymbol{X}_j \approx r\alpha_j e^{i\theta_j} \sim \boldsymbol{r}_j$. Neglecting terms of order $(1/N)$, it just corresponds to $\alpha_i \leftrightarrow \alpha_j$ and $\theta_i \leftrightarrow \theta_j$. The derivation of the transformation rules, including terms of order $(1/N)$, is straightforward but tedious. Just as for $N = 3$, however, it turns out in what follows that we do not need to consider individual $i \leftrightarrow j$ transformations.

3.1. The spin-polarized system

Consider the classical configuration Ω_0' shown in figures 4 and 5. For large j the electrons can be thought of as forming an approximately ring-like structure. Counting the number of rings from the centre outwards, the first ring contains 6 electrons, the second contains approximately 12 and so on. We first focus on a 'typical' ring without any defects; it will contain a large, even number N_m of electrons (approximately $6m$ electrons where $6m \gg 1$), but these electrons will have an index $j \gg 1$, i.e. we are not considering rings near the edge of the N-electron droplet. We are going to consider just the subset of all particle interchanges $i \leftrightarrow j$ which are equivalent to rotations of this mth ring. Since $\boldsymbol{X}_j \approx r\alpha_j e^{i\theta_j} \sim \boldsymbol{r}_j$, all members of the ring have approximately the same α, i.e. $\{\alpha_j\} \equiv \alpha_m$ for all j in ring m. Hence interchanging two members of the ring just involves a transformation between their θ_j-coordinates. Since all members of the ring have a similar environment and the same α_j, the potential energy w_j and hence g_j in equation (26) will have the same form for all j in the ring m. As for $N = 3$, the lowest-energy solutions should be those with g_j nodeless; g_j will be an approximately gaussian function of $\theta_{[j]}$ centred at $\theta_{[j0]}$. Hence we can write $g_j \equiv g_m$ for all j in ring m. We now rotate the electrons in the ring, and hence the ring itself, by an angle $2\pi/N_m$. Since $\boldsymbol{X}_j \sim \boldsymbol{r}_j$ this corresponds to $\theta_j \to \theta_j + 2\pi/N_m$. The g_m functions are nodeless and (in a given ring) identical, and hence the product $\prod_j g_j(\theta_{[j]} - \theta_{[j0]})$ for j in ring m can be replaced by $\prod_j g_m(\theta_{[j]} - \theta_{[j0]})$. The transformation keeps the system within the subset of all SEMs corresponding to the same ring ordering, i.e. just as for $N = 3$ the rotation operation in real space becomes a space-group operation in Ω' space which translates the system between SEMs. Recall that $G(\Omega')$ for minimum-energy states should resemble a 'bonding' linear combination of s-like orbitals (i.e. an approximately gaussian θ-dependence around the various SEMs (equation (28))). The coefficients $c_{i;a}$ in the expression for $G(\Omega')$

in equation (28) will therefore be identical for all of the SEM minima $\{\Omega_i'\}$ corresponding to this same ring ordering. Since $G(\Omega')$ corresponds to a linear combination of identical orbitals with the same coefficient, the overall effect of the transformation on $G(\Omega')$ due to ring rotation will be quite small; we simply move between this subset of SEMs $\{\Omega_i'\}$, each of which has the same local orbitals. In contrast, the effect on the θ'-variable is relatively important; it follows from equation (8) that $\theta_j \rightarrow \theta_j + 2\pi/N_m$ corresponds to $\theta' \rightarrow \theta' + \Delta\theta'$, where

$$\Delta\theta' = N_m \frac{2\pi}{N_m(N-1)} = \frac{2\pi}{(N-1)}.$$

The total function $F(\Omega) = \mathrm{e}^{\mathrm{i}J\theta'}G(\Omega')$ hence becomes $\mathrm{e}^{\mathrm{i}J\Delta\theta'}F(\Omega)$. Given that N_m is an even number, rotation of the mth ring by $2\pi/N_m$ necessarily corresponds to an odd number of interchanges $i \leftrightarrow j$. If we assume that the electrons are *spin polarized*, the spatial part of the N-electron wavefunction must be totally antisymmetric, and hence the overall phase change must equal $\mathrm{e}^{\mathrm{i}\pi(2n+1)}$ where n is any integer. Denoting the J-value as J_{WX}, we therefore obtain the condition

$$J_{WX} = \frac{1}{2}(N-1)(2n+1). \tag{29}$$

Importantly, this criterion for J_{WX} is *independent* of m, and hence holds for all rings m. In other words, this criterion guarantees that the N-electron wavefunction has the correct permutational symmetry under the subset of all permutations of N electrons which correspond to ring rotations. Note that J_{WX} must be an integer.

Now consider the Wigner crystal plus defect (WXD). Fisher, Halperin and Morf [26] showed that the lowest-energy defect states correspond to interstitial defects, i.e. an extra electron sits on an interstitial site in the otherwise perfect crystal. Single vacancies have a higher energy. Following Fisher *et al*, there are two types of interstitial site, 'centred' and 'edge' interstitials, and these are by far the most predominant type of defect at finite temperatures. In our model, these defects can be created by introducing an $(N+1)$th electron which forms the defect. There are several reasons for this being reasonable. First, the alternative scheme of allowing one of the N existing electrons to form the defect would create an interstitial *plus* vacancy; following Fisher *et al* the total energy of such a defect is approximately three times larger than a single interstitial. Second, creation of such an interstitial–vacancy pair would involve a transformation of both θ- *and* α-coordinates within the N-electron Ω space. Third, the definition of the $\theta_{[j]}$-variables (see equation (9)) is independent of the coordinates of electron $N+1$. Hence the N-electron Ω' coordinate system is essentially unchanged by the presence of the extra electron. The hyperangular function $G(\Omega')$ for the N-electron system can therefore be compared directly to the corresponding hyperangular function for the $(N+1)$-electron system when projected onto the N-electron Ω' space. We wish to consider the effect of this defect on ring m. Following Fisher *et al* [26], the distortion of the crystal will be well localized around the defect. In terms of the hyperangular coordinates, part of the local crystal distortion will be subsumed in the coordinate r, and the effect on the hyperangles α and θ of the electrons in ring m will be relatively small unless the defect lies in ring m. Assume that the defect lies in ring $m = m_d$. The antisymmetry condition obtained above for the perfect crystal (J_{WX}) will still be approximately valid for all rings with $m \neq m_d$. In ring m_d, there are now an *odd* number of electrons $N_m + 1$. The rotation $\theta_j \rightarrow \theta_j + 2\pi/(N_m+1)$ now corresponds to $\theta' \rightarrow \theta' + \Delta\theta'$ where

$$\Delta\theta' = (N_m+1)\frac{2\pi}{(N_m+1)N} = \frac{2\pi}{N}$$

(NB we now have an $(N+1)$-electron system). Because of the odd-member ring, rotation corresponds to an even number of $i \leftrightarrow j$ interchanges. The hyperangular function for the $(N+1)$-electron system of crystal plus defect, when projected onto the original N-electron Ω' space, is essentially unchanged—the original N electrons are only slightly distorted by the presence of the defect. Hence the overall phase change $e^{iJ\Delta\theta'}$ must equal $e^{i2\pi n'}$, where n' is any integer. Denoting the J-value as J_{WXD}, we therefore obtain the condition

$$J_{WXD} = Nn'. \tag{30}$$

Again, this criterion for J_{WXD} is *independent* of m, and hence holds for a single defect located in any ring m. Also, J_{WXD} must be an integer. These two criteria, taken together, therefore guarantee that the N-electron wavefunction has the correct permutational symmetry under the subset of all permutations of N electrons which correspond to ring rotations, both for the perfect crystal (WX) *and* the crystal plus defect (WXD). For the perfect crystal, we can consider N to be odd since each ring contains an even number of electrons, plus there is one electron at the centre. Combining the two conditions for J_{WX} and J_{WXD}, we hence see that the WX and WXD have the following common J-values:

$$J_m = \frac{1}{2}N(N-1)(2n+1) \tag{31}$$

where n is any integer. Converting these J_m-values into filling factors using the formula $\nu = N(N-1)/2J_m$, which is valid for large N, yields

$$\nu = \frac{1}{2n+1}. \tag{32}$$

This coincides with the principal series of FQHE fractions, i.e. $\frac{1}{3}$ and $\frac{1}{5}$. The value $\nu = 1$ will be discussed below. As an illustration we consider the case of $N = 201$ electrons. The allowed J_{WX}-values are 100×1, 100×3, 100×5, etc, while the allowed J_{WXD}-values are 201×1, 201×2, 201×3, etc. It is clear that common J-values are given by $J_m = 100 \times 201 \times 1$, $100 \times 201 \times 3$, etc, and hence $\nu = \frac{1}{3}, \frac{1}{5}$.

3.2. The spin-unpolarized system

We have so far generated the J_m-values for a system of spin-polarized particles. Next we consider the opposite limit of a spin-unpolarized system, i.e. $N_+ = N_-$ where $N = N_+ + N_-$, and N must therefore be an even number. The arguments will be more approximate in this case, but we believe will still contain the essential physics. Consider a 'typical' ring as before. Let this ring, m, contain N_m electrons where $N_m \gg 1$; the ring will typically have $N_m/2$ up-spins and $N_m/2$ down-spins. Due to the Pauli principal keeping like spins apart, we will assume that on the average the ordering corresponds to the alternating sequence up-spin–down-spin repeated around the ring (see figure 6(a)). Rotation of the ring to a topologically identical configuration now involves a rotation of all of the electrons in the ring by an angle $2\pi/(N_m/2)$, i.e. we have to rotate through twice $2\pi/N_m$. The rotation $\theta_j \to \theta_j + 2\pi/(N_m/2)$ corresponds to $\theta' \to \theta' + \Delta\theta'$ where

$$\Delta\theta' = N_m \frac{2\pi}{(N_m/2)(N-1)} = \frac{4\pi}{(N-1)}.$$

Since N_m is an even number, $N_m/2$ can either be odd or even. Rotation of the mth ring by $4\pi/N_m$ therefore corresponds to either an even or odd number of interchanges $i \leftrightarrow j$ for *both* spin-up and spin-down electrons. Hence the total number of interchanges of *like*

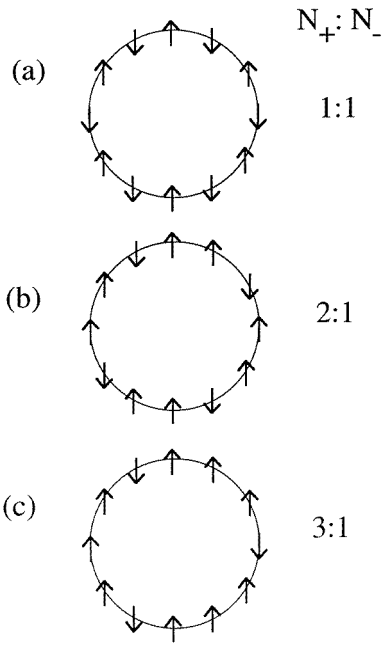

Figure 6. A typical ring m for the various spin polarizations. Although only 12 particles are shown for clarity, the ring is assumed to contain a large number, i.e. $N_m \gg 1$ since $m \gg 1$. (a) N_+:N_- = 1:1. (b) N_+:N_- = 2:1. (c) N_+:N_- = 3:1.

spins is always even. The overall phase change must therefore equal $e^{i2\pi n}$ where n is any integer. Denoting the J-value as J_{WX} we therefore obtain the condition

$$J_{WX} = \frac{1}{2}(N-1)n. \tag{33}$$

Again this criterion for J_{WX} is independent of m, and hence holds for all rings m. Now consider the Wigner crystal plus defect (WXD) with the defect in ring m. The defect corresponds to an extra electron which can either be spin-up or spin-down. There are now an *odd* number of electrons, $N_m + 1$. We now have, for large N_m, that

$$\Delta\theta' \approx 2(N_m+1)\frac{2\pi}{(N_m+1)N} = \frac{4\pi}{N}$$

for the $N+1$ electron system. Because of the odd-member ring, rotation now corresponds to an overall *odd* number of $i \leftrightarrow j$ interchanges. This is because either the spin-up interchanges are odd while the spin-down ones are even, or vice versa. Hence the overall phase change $e^{iJ\Delta\theta'}$ must equal $e^{i\pi(2n'+1)}$, where n' is any integer. Denoting the J-value as J_{WXD}, we therefore obtain the condition

$$J_{WXD} = \frac{1}{2}N\left(n' + \frac{1}{2}\right). \tag{34}$$

Again, this criterion for J_{WXD} is independent of m. These two criteria, taken together, therefore guarantee that the spin-unpolarized N-electron wavefunction has the correct permutational symmetry under the subset of all permutations of N electrons which correspond to ring rotations, both for the perfect crystal (WX) *and* the crystal plus defect

(WXD). Combining the two conditions for integer values of J_{WX} and J_{WXD}, we hence see that the WX and WXD have the following common J-values:

$$J_m = \frac{1}{4}N(N-1)(2n+1) \tag{35}$$

where n is any integer. Converting these J_m-values into filling factors yields

$$\nu = \frac{2}{2n+1}. \tag{36}$$

This coincides with the second series of FQHE fractions, i.e. $\frac{2}{3}$, $\frac{2}{5}$, $\frac{2}{7}$, etc, and hence suggests that the ground states at these fractions will be spin unpolarized in the absence of Zeeman energy, in agreement with earlier finite-size numerical calculations (see p 63 of reference [3]). Interestingly the series also reproduces the IQHE value $\nu = 2$. As an illustration we consider the case of $N = 200$ electrons. The allowed J_{WX}-values are 199×1, 199×2, 199×3, etc, while the allowed J_{WXD}-values are 50×1, 50×3, 50×5, etc. Common J-values are given by $J_m = 199 \times 50 \times 1$, $199 \times 50 \times 3$, etc, and hence $\nu = \frac{2}{3}, \frac{2}{5}$, etc.

3.3. The partially spin-polarized system

Consider a partially spin-polarized system. First we will take $N_+ = 3N_-$, where $N = N_+ + N_-$ and N is again even. Consider a 'typical' ring as before. Let this ring, m, contain N_m electrons where $N_m \gg 1$; the ring will typically have $3N_m/4$ up-spins and $N_m/4$ down-spins. Due to the Pauli principle keeping like spins apart, we will now assume that on average the ordering corresponds to the sequence up-spin–up-spin–up-spin–down-spin repeated around the ring (see figure 6(c)). Rotation of the ring to a topologically identical configuration now involves a rotation of all of the electrons in the ring by an angle $2\pi/(N_m/4)$, i.e. we have to rotate through four times $2\pi/N_m$. The rotation $\theta_j \to \theta_j + 2\pi/(N_m/4)$ corresponds to $\theta' \to \theta' + \Delta\theta'$, where

$$\Delta\theta' = N_m \frac{2\pi}{(N_m/4)(N-1)} = \frac{8\pi}{(N-1)}.$$

Since N_m is an even number, $3N_m/4$ and $N_m/4$ are either both odd or both even. Rotation of the mth ring by $8\pi/N_m$ therefore corresponds to either an even or odd number of interchanges $i \leftrightarrow j$ for *both* spin-up and spin-down electrons. Hence the total number of interchanges of *like* spins is always even. The overall phase change must therefore equal $e^{i2\pi n}$, where n is any integer. Denoting the J-value as J_{WX}, we therefore obtain the condition

$$J_{WX} = \frac{1}{4}(N-1)n. \tag{37}$$

Again this criterion for J_{WX} is independent of m, and hence holds for all rings m. Now consider the Wigner crystal plus defect (WXD) with the defect in ring m. The defect can either be spin-up or spin-down. There are now an *odd* number of electrons $N_m + 1$. We now have, for large N_m, that

$$\Delta\theta' \approx 4(N_m+1)\frac{2\pi}{(N_m+1)N} = \frac{8\pi}{N}$$

for the $(N+1)$-electron system. Because of the odd-member ring, rotation now corresponds to an overall *odd* number of $i \leftrightarrow j$ interchanges. This is because either the spin-up interchanges are odd while the spin-down ones are even, or vice versa. Hence the overall

phase change $e^{iJ\Delta\theta'}$ must equal $e^{i\pi(2n'+1)}$, where n' is any integer. Denoting the J-value as J_{WXD}, we therefore obtain the condition

$$J_{WXD} = \frac{1}{4}N\left(n' + \frac{1}{2}\right). \tag{38}$$

Again, this criterion for J_{WXD} is independent of m. These two criteria, taken together, therefore guarantee that the partially spin-polarized N-electron wavefunction has the correct permutational symmetry under the subset of all permutations of N electrons which correspond to ring rotations, both for the perfect crystal (WX) *and* the crystal plus defect (WXD). Combining the two conditions for integer values of J_{WX} and J_{WXD}, we hence see that the WX and WXD have the following common J-values:

$$J_m = \frac{1}{8}N(N-1)(2n+1) \tag{39}$$

where n is any integer. Converting these J_m-values into filling factors yields

$$\nu = \frac{4}{2n+1}. \tag{40}$$

This coincides with the fourth series of FQHE fractions, i.e. $\frac{4}{5}$, $\frac{4}{7}$, etc, and hence the theory suggests that the corresponding ground states at these fractions will be partially spin polarized in the ratio of spin-up to spin-down of 3:1 in the absence of Zeeman energy. Again this is in agreement with finite-size numerical calculations (see p 63 of reference [3]). As an illustration we again consider the case of $N = 200$ electrons (NB we have 4 as a factor since the ratio of spin-up to spin-down is 3:1). The allowed J_{WX}-values are 199×1, 199×2, 199×3, etc, while the allowed J_{WXD}-values are 25×1, 25×3, 25×5, etc. Common J-values are given by $J_m = 199 \times 25 \times 1$, $199 \times 25 \times 3$, etc, and hence $\nu = \frac{4}{5}$, $\frac{4}{7}$, etc.

Next we take $N_+ = 2N_-$, where $N = N_+ + N_-$ and N is again even. Consider a 'typical' ring as before. Let this ring, m, contain N_m electrons where $N_m \gg 1$; the ring will typically have $2N_m/3$ up-spins and $N_m/3$ down-spins. Due to the Pauli principle keeping like spins apart, we will assume that on average the sequence corresponds to up-spin–up-spin–down-spin repeated around the ring (see figure 6(b)). Rotation of the ring to a topologically identical configuration now involves a rotation of all of the electrons in the ring by an angle $2\pi/(N_m/3)$, i.e. we have to rotate through three times $2\pi/N_m$. The rotation $\theta_j \to \theta_j + 2\pi/(N_m/3)$ corresponds to $\theta' \to \theta' + \Delta\theta'$, where

$$\Delta\theta' = N_m \frac{2\pi}{(N_m/3)(N-1)} = \frac{6\pi}{(N-1)}.$$

Since N_m is an even number, $2N_m/3$ and $N_m/3$ are either both odd or both even. Rotation of the mth ring by $6\pi/N_m$ therefore corresponds to either an even or an odd number of interchanges $i \leftrightarrow j$ for *both* spin-up and spin-down electrons. Hence the total number of interchanges of *like* spins is always even. The overall phase change must therefore equal $e^{i2\pi n}$, where n is any integer. Denoting the J-value as J_{WX}, we therefore obtain the condition

$$J_{WX} = \frac{1}{3}(N-1)n. \tag{41}$$

Again this criterion for J_{WX} is independent of m, and hence holds for all rings m. Now consider the Wigner crystal plus defect (WXD) with the defect in ring m. The defect can

either be spin-up or spin-down. There are now an *odd* number of electrons $N_m + 1$. We now have, for large N_m, that

$$\Delta\theta' \approx 3(N_m + 1)\frac{2\pi}{(N_m + 1)N} = \frac{6\pi}{N}$$

for the $(N+1)$-electron system. Because of the odd-member ring, rotation now corresponds to an overall *odd* number of $i \leftrightarrow j$ interchanges. This is because either the spin-up interchanges are odd while the spin-down ones are even, or vice versa. Hence the overall phase change $e^{iJ\,\Delta\theta'}$ must equal $e^{i\pi(2n'+1)}$, where n' is any integer. Denoting the J-value as J_{WXD} we therefore obtain the condition

$$J_{WXD} = \frac{1}{3}N\left(n' + \frac{1}{2}\right). \tag{42}$$

Again, this criterion for J_{WXD} in independent of m. These two criteria, taken together, therefore guarantee that the partially spin-polarized N-electron wavefunction has the correct permutational symmetry under the subset of all permutations of N electrons which correspond to ring rotations, both for the perfect crystal (WX) *and* for the crystal plus defect (WXD). Combining the two conditions for integer values of J_{WX} and J_{WXD}, we hence see that the WX and WXD have the following common J-values:

$$J_m = \frac{1}{6}N(N-1)(2n+1) \tag{43}$$

where n is any integer. Converting these J_m-values into filling factors yields

$$\nu = \frac{3}{2n+1}. \tag{44}$$

This coincides with the third series of FQHE fractions, i.e. $\frac{3}{5}$, $\frac{3}{7}$, etc, and predicts the corresponding ground states to be partially spin polarized in the ratio of spin-up to spin-down of 2:1 (or vice versa) in the absence of Zeeman energy. We note that there is an alternative system that also yields the filling factor series $\nu = 3/(2n+1)$. In particular, this fraction emerges from considering a fully spin-polarized system, but now considering rotation of two rings simultaneously. These two states with N_+:N_- = 2:1 and $N_- = 0$, respectively, probably compete to become the ground state depending on the value of the Zeeman energy (and hence magnetic field). Interestingly, finite-size studies have shown that the $\nu = \frac{3}{5}$ state is indeed partially polarized for $B < 15$ T in the ratio N_+:N_- = 2:1, but fully polarized for $B > 15$ T (see p 160 of reference [3]).

The above arguments can be extended straightforwardly to consider $N_+ = (p-1)N_-$, where $N = N_+ + N_-$ and p is any integer. In this case, the corresponding filling fraction becomes $\nu = p/(2n+1)$. We now focus on the filling factor $\nu = 1$ (IQHE). We have already shown that this state emerges from the two following series: $\nu = 1/(2n+1)$ for $n = 0$ in a fully spin-polarized system, or $\nu = 3/(2n+1)$ for $n = 1$ in a partially spin-polarized system. In fact, for a given spin polarization $N_+ = (p-1)N_-$ with p odd, the factor $\nu = 1$ will always arise, i.e. by choosing $n = (p-1)/2$. It is reasonable to expect these states to compete to become the ground state. This is consistent with recent findings that a gap exists at $\nu = 1$ (IQHE) even in the *absence* of Zeeman splitting. The possible coexistence of a manifold of partially spin-polarized states is also consistent with the idea of macroscopic spin textures near $\nu = 1$; in particular, taking a linear combination of partially spin-polarized states enables the construction of localized 'wave-packets' of spin to be carried out—we conjecture that the resulting spin textures may be related to skyrmions.

We note that the above filling factors emerged from requiring that the WX and WXD had a common angular momentum value. The defect was considered to be an interstitial electron. It turns out that, as far as the common J_m-values are concerned, we could also have considered the defect to be a vacancy. The product $(N-1)(N-2)$ would have appeared throughout this section instead of $N(N-1)$; in the large-N limit, both products yield $\sim N^2$ and hence the same filling factors. Hence at $J = J_m$, the WX can coexist with a WXD where the defect is either an interstitial electron or a vacancy. As noted earlier, however, such vacancies do have a higher energy, and hence are less likely to occur at finite temperatures.

3.4. Analytic calculation of FQHE energy gaps

In this section we will give an analytic calculation for the energy gaps associated with the FQHE and IQHE states, i.e. for $J = J_m$. The calculation is approximate since it relies on the various approximations made in section 2.3. However, our goal is to find whether the gaps predicted by our model are in fact consistent with the observed FQHE gaps, and also to identify trends in the energy gaps with filling fraction, magnetic field, etc.

In section 2.3, we obtained an approximate expression for the relative energy $E_{\rm rel}$ (see equation (27)). This energy depends on E_α and E_θ. In section 3, we argued that the important criterion characterizing the magic-number J-values was that the crystal (WX) and defect (WXD) can both have the same J-value, given by $J = J_m$; this leads to a large delocalization energy due to increased WX–WXD tunnelling in Ω' space. In the language of single-particle tight-binding theory, the resulting energy gap between states with $J = J_m$ and $J \neq J_m$ arises from the hybridization of the $G(\Omega')$ solutions peaked around, for example, Ω'_0 and $\Omega'_{0;a}$ at $J = J_m$. This hybridization hence yields a low $E_{\rm rel}$ because of the corresponding delocalization of $G(\Omega')$ at $J = J_m$, i.e. a reduction in zero-point energy. Here we will obtain an analytic expression for this energy using a simple model for the effect of delocalization, and show that the resulting gaps are consistent with experimental findings.

As pointed out earlier, a state of a given negative J will have an energy minimum at a finite magnetic field ω_c. As ω_c increases, the value of J at which the energy $E_{\rm rel}(J)$ has a minimum will increase. We will calculate the energy difference between a state with $J = J_m$ and competing low-energy states with J given by $J_{m\pm} = J_m \pm \delta$ at a given ω_c, where $\delta \ll J_m$. The lowest-energy state with $J = J_m$ is given by equation (27) with $n = 0$:

$$E_{\rm rel}(J_m) = \hbar\omega_0(B)\left[\left([N-2]^2 + J_m^2 + \frac{2m^*\beta}{\hbar^2}V(\Omega'_0) + \frac{2m^*}{\hbar^2}[E_\theta(J_m) + E_\alpha(J_m)]\right)^{1/2} + 1\right] - J_m\frac{\hbar\omega_c}{2} \tag{45}$$

while that with $J = J_{m\pm}$ is given by

$$E_{\rm rel}(J_{m\pm}) = \hbar\omega_0(B)\left[\left([N-2]^2 + [J_m \pm \delta]^2 + \frac{2m^*\beta}{\hbar^2}V(\Omega'_0) + \frac{2m^*}{\hbar^2}[E_\theta(J_{m\pm}) + E_\alpha(J_{m\pm})]\right)^{1/2} + 1\right] - [J_m \pm \delta]\frac{\hbar\omega_c}{2}. \tag{46}$$

As discussed in section 2.1, the angular momentum is negative for low-lying energy states; hence we have included the minus sign directly into these expressions, i.e. J_m and $J_{m\pm}$

are positive numbers. Consider the state with $J = J_m$. This state can coexist as both a crystal (WX) and a crystal plus defect (WXD), in contrast to the state $J_{m\pm}$. The transition WX→WXD will involve a distortion of the Ω' coordinates. This distortion in Ω' space corresponds to a spreading or 'delocalization' of the function $G(\Omega')$ along these directions. There is therefore a reduction in 'localization' energy going from a state with $J \neq J_m$ (i.e. WX and WXD cannot coexist) to a state with $J = J_m$ (i.e. WX and WXD can coexist). We will hence write

$$E_\theta(J_m) + E_\alpha(J_m) + \beta V(\Omega'_0) = E_0 \tag{47}$$

while

$$E_\theta(J_{m\pm}) + E_\alpha(J_{m\pm}) + \beta V(\Omega'_0) = E_0 + \tilde{\Delta} \tag{48}$$

where $\tilde{\Delta}$ represents the increased localization energy of state $J_{m\pm}$ as compared to J_m. Note that the potential energy minimum $\beta V(\Omega'_0)$ is a constant term throughout. In the appendix, we show that typically $\tilde{\Delta} \sim N^2$, while $E_0 \sim N^3$. Hence in the limit of $N \gg 1$, we have $E_0 \gg \tilde{\Delta}$. We also recall from section 3 that $J_m \sim N^2$. It follows by expanding out equations (45) and (46) in the limit $N \gg 1$ that

$$\Delta E_\nu \equiv E_{\rm rel}(J_{m\pm}) - E_{\rm rel}(J_m) \approx \overline{h}\omega_0(B)\left[\frac{m^*\tilde{\Delta}/\overline{h}^2 \pm J_m\delta}{[J_m^2 + 2m^*E_0/\overline{h}^2]^{1/2}}\right] \mp \delta\frac{\overline{h}\omega_c}{2}. \tag{49}$$

We are interested in the large-N limit, since our goal is to calculate the FQHE gaps; hence we will choose the confinement $\omega_0 \ll \omega_c$, which yields $\omega_0(B) \sim \omega_c/2$. Let us first consider the filling factor $\nu = \frac{1}{3}$, and hence $J_m = 3N(N-1)/2$. Substituting into equation (49), we obtain the approximate expression for the energy gap:

$$\Delta E_{1/3} \sim \frac{1}{3}\frac{m^*\tilde{\Delta}}{N^2\overline{h}^2}\overline{h}\omega_c. \tag{50}$$

There are several points to note about this expression for the energy gap at $\nu = \frac{1}{3}$.

(i) Given that $\tilde{\Delta} \sim N^2$ for large N, the expression is *independent* of the electron number N. It is also independent of the strength of the parabolic potential ω_0. For a given ω_c corresponding to the filling factor $\nu = \frac{1}{3}$, we can therefore take the thermodynamic limit $N \to \infty$ and yet still maintain a *fixed* average electron density by choosing appropriately small values of ω_0. Our expression for the energy gap at filling factor $\nu = \frac{1}{3}$, which was derived in terms of J-values for a fixed-N system, therefore also holds for an infinite two-dimensional electron gas of fixed density.

(ii) The expression for the energy gap does not exhibit a direct dependence on the value of the electron–electron interaction β. We do emphasize, however, that throughout most of this paper we have *assumed* that β is large enough for us to be able to neglect tunnelling between SEMs. Hence we can only conclude that the absolute value of β does not directly affect the energy gap ΔE for sufficiently large β. This is consistent with experimental findings that the gap can be remarkably sample independent [3]. Below we will mention how a weak dependence on β will arise if one considers smaller values of β.

(iii) The energy gap appears to be approximately *linear* in the magnetic field. Most previous theoretical studies conclude that the dependence resembles $B^{1/2}$. As we will show below, the linear dependence is in reasonable agreement with experimental data, particularly at lower fields. However, we will later discuss how a weaker, non-linear dependence, i.e. B^x where $x < 1$, can eventually arise at larger B in our model.

(iv) The energy gap does not depend on δ to first order in (δ/J_m). This independence of δ is important since it implies that the energy gap exists between state J_m and *all* other

states with J in the vicinity of J_m. We know from the discussion at the end of section 2.1 that, over a given range of magnetic field, the states which compete to become the ground state will be those of similar J. Hence we expect the energy gap arising to exist over a small but finite range of magnetic field, as observed experimentally.

(v) The expression for the gap ΔE can be made applicable to situations where the lowest-energy excitation involves spin flips, by adding $\Delta E_{\rm spin}$, where $\Delta E_{\rm spin}$ is the difference in total spin energy between the excited state and the $\nu = \frac{1}{3}$ spin-polarized ground state. We are interested in the lowest-energy excitations with $\Delta E_{\rm spin} = 0$; $\Delta E_{\rm spin} \geqslant 0$ for the fully spin-polarized initial state at $\nu = \frac{1}{3}$. For other fractions, the term $\tilde{\Delta}$ will have an indirect dependence on the spin configuration since, for a mixed spin system, the Ω' space is really coupled to the spinor space by the antisymmetry condition, and hence $G(\Omega')$ is actually a two-dimensional vector. A detailed discussion of spin-reversed excited states will be given elsewhere.

(vi) Given the discussion in (v), together with the fact that $\tilde{\Delta}$ has a weak but finite dependence on J_m (see later), we can conclude the value of $\tilde{\Delta}$ will generally be different for different fractions. Gaps at other fractions in the $\nu = p/3$ series are discussed below.

We will now attempt to derive an approximate analytic expression for $\tilde{\Delta}$. Consider the N-electron system at $J = J_m$. As discussed in section 3, the system can exist as both a crystal (WX) and a crystal plus defect (WXD), in contrast to the state $J_{m\pm}$. We will argue in what follows that the transition WX$\rightarrow$WXD involves a significant fractional distortion of θ-coordinates. This distortion along the $\{\theta_{[j]}\}$-axes in Ω' space corresponds to a spreading or 'delocalization' of the function $G(\Omega')$ along these directions, thereby giving rise to a finite $\tilde{\Delta}$. In sections 2 and 3, we argued that the low-energy SIMs near a given SEM consisted of a single-electron defect placed at an interstitial site within the hexagonal crystal. As noted at the end of section 3, the defect could also be a vacancy, although the corresponding SIM would have a higher energy. Consider a defect placed in ring m which contains N_m particles with $N_m \gg 1$, and let the defect be sited between j and $j+1$ (cf. figure 5). Classically, the system moves to a nearby SIM in Ω' space (cf. figure 2). In particular, the defect will cause a distortion of the coordinates of particle j. In order to calculate the maximum possible distortion (and hence delocalization available as a result of the hybridization between the SEM and SIM), we will consider the particular SIM in which only particle j moves to accommodate the defect. In principle, both the α_j- and $\theta_{[j]}$-coordinates will be modified, thereby 'sharing' the effect of the distortion. However, with the defect placed between j and $j+1$ in ring m, the distortion of particle j will mainly be along the $\theta_{[j]}$-direction. The idea that the most important effect of the defect is the distortion of the θ-coordinates is consistent with the following considerations. Consider any particle j' near to the defect with coordinates $\theta_{[j']}$ and $\alpha_{j'}$. Let the nearby defect cause a distortion of a in all directions. Hence the new coordinates of the particle j' are approximately $\alpha_{j'} + a$ and $\theta_{[j']} + a/\alpha_{j'}$. The relative distortion caused by the nearby defect is hence $\Delta\alpha_{j'}/\alpha_{j'} \sim a/\alpha_{j'}$, while $\Delta\theta_{[j']}/\theta_{[j']} \sim a/(\alpha_{j'}\theta_{[j']})$. For $N \gg j'$, $\alpha_{j'}$ changes slowly with j', and is unchanged if j' lies in ring m. However, $\theta_{[j']}$ ranges from 0 to 2π within ring m, and hence the fractional change $\Delta\theta_{[j']}$ can be significant.

We will therefore consider $\tilde{\Delta}$ as arising as a result of the difference in E_θ for J_m as compared to $J_{m\pm}$. The loss of 'localization' energy of the state J_m as compared to $J_{m\pm}$ can be significant along the $\{\theta_{[j]}\}$ directions, i.e. E_θ can differ appreciably depending on whether the function $G(\Omega')$ is localized (i.e. $J = J_{m\pm}$) or not ($J = J_m$). Consider equation (26) for the 'energy' e_j associated with a particle j in ring m where $J \neq J_m$ (i.e. WX and WXD cannot coexist). The equation resembles a one-dimensional Schrödinger equation in $\theta_{[j]}$ for

a mass α_{j0} moving in a potential $w_j(\theta_{[j]} - \theta_{[j0]})$. The function w_j will have a minimum at $\theta_{[j]} = \theta_{[j0]}$, whereas there are maxima at $\theta_{[j]} = \theta_{[j0]} \pm 2\pi/N_m$ as particle j approaches particle $j \pm 1$. For $N = 3$, recall figure 3, where moving along the y-axis (θ-axis) at fixed $\alpha = \alpha_0$ (i.e. $x = 0$) produced a minimum at $y = 0$ and maxima at $y = \pm\pi/2$. We can approximate e_j using a simple one-dimensional particle-in-a-box model: we will assume that w_j is a flat-bottomed potential with infinite walls at $\theta_{[j]} = \theta_{[j0]} \pm 2\pi/N_m$. The width of the box is therefore given by $a_j = 4\pi/N_m$. The energy $e_j^{(J)}$ is hence approximately given by

$$e_j^{(J)} \sim \frac{\hbar^2\pi^2 N_m^2}{2m^*\alpha_{j0}^2[4\pi]^2}. \tag{51}$$

Note that the width of the wavefunction g_j, and hence the localization of $G(\Omega')$ along $\theta_{[j]}$, is characterized by a_j. This expression (equation (51)) for $e_j^{(J)}$ implicitly assumes that the electron–electron interaction β is large; for smaller values of β, the particle-in-a-box energy should pick up a weak dependence on β. Throughout this paper, however, we will use the approximate analytic form given in equation (51). At $J = J_m$, there is distortion of $G(\Omega')$, since WX and WXD can coexist. The defect can occupy any interstitial site in the crystal; each defect position produces a distinct SIM. There exists a SIM (e.g. $\Omega'_{0;j}$) in which the defect is placed next to particle j, say between particles j and $j+1$ as used earlier. We can see that there is one such SIM associated with each $\theta_{[j]}$-coordinate. If, as discussed above, we consider the main distortion as occurring on the $\theta_{[j]}$-coordinate of particle j, then the associated SIM lies on the $\theta_{[j]}$-axis. In this case the coexistence of the SEM Ω'_0 and the SIM $\Omega'_{0;j}$ causes an increase in the effective box width, $a_j \to a_j + \delta a_j$. The energy along the $\theta_{[j]}$-direction is now given by

$$e_j^{(Jm)} \sim e_j^{(J)} + \frac{\partial e_j^{(J)}}{\partial a_j}\delta a_j \sim e_j^{(J)}\left[1 - 2\frac{\delta a_j}{a_j}\right]. \tag{52}$$

Although there are many such SIMs associated with each SEM, we know that the defects have a low density at the temperatures of interest. The system also requires a large time to tunnel between these SIMs, since each SIM describes a different defect position in the crystal; diffusion of the defect between sites will be slow at low temperatures. It is reasonable therefore to suppose that each SEM hybridizes with just one of these SIMs at any time. The average loss of localization energy of state J_m as a result of distortion due to a nearby SIM is therefore obtained by averaging over all $(N-2)$ $\theta_{[j]}$-coordinates. Hence, using equation (52),

$$\tilde{\Delta} \sim \frac{1}{N-2}\sum_j 2\left[\frac{\delta a_j}{a_j}\right]e_j^{(J)} \sim 2\overline{\left[\frac{\delta a}{a}\right]}\bar{e} \tag{53}$$

where $\bar{x}$ represents an average of the quantity x over all $(N-2)$ of the $\theta_{[j]}$-coordinates.

We could also try to obtain expressions for ΔE at other fractions. Consider $\nu = \frac{1}{5}$. Equation (50) now has the factor $\frac{1}{3}$ replaced by $\frac{1}{5}$. Assuming as a crude approximation that the values of $\tilde{\Delta}$ are the same, we obtain the result that $\Delta E_{1/5}{:}\Delta E_{1/3} \sim 0.6$ for samples at a given magnetic field. The literature tends to put this ratio at about 0.3–0.4 [27, 28]. One could also try to evaluate ΔE for other fractions where the ground state J_m and/or the excited states $J_{m\pm}$ are thought to have spin-reversed electrons. Such a calculation needs a more careful estimation of $\tilde{\Delta}$, as discussed earlier. Here we will just provide a rough estimate by considering, as before, excitations which do not change the total spin component (i.e. $\Delta E_{\text{spin}} = 0$). We will choose $\nu = \frac{2}{3}$ in order to compare with the results

for $\nu = \frac{1}{3}$. There are two effects of considering $\nu = \frac{2}{3}$ instead of $\nu = \frac{1}{3}$ when re-deriving the expressions obtained in this section. The prefactor in equation (50) increases by a factor of 2, while $\delta a_j/a_j$ decreases by a factor of 2. This decrease in $\delta a_j/a_j$ arises as follows. Recall that like spins in the spin-unpolarized case are separated by twice the angle of the spin-polarized case. The 'unit-cell' size in Ω' space is determined by the separation between neighbouring SEMs, and is therefore twice as large for the unpolarized case. The effective box size must therefore also be twice as large, i.e. the effective a_j-value is now $8\pi/N_m$ instead of $4\pi/N_m$. Hence the final result is that $\Delta E_{2/3} \sim \Delta E_{1/3}$. Although we do not attach too much importance to this result because of the complications of spin, it is interesting to note that experimentally the gaps for $\nu = \frac{1}{3}$ and $\nu = \frac{2}{3}$ are found to be similar [3, 27, 28], as will be shown below. We note that allowing for spin-flip excitations at $\nu = \frac{2}{3}$ may reduce the overall gap at low B, since ΔE_{spin} can be negative if the ground state is not fully spin polarized. Hence the total gap may be negligible for $\nu = \frac{2}{3}$ at low B. This feature is also seen experimentally. The same argument concerning effective box size should also be approximately true for the other partially spin-polarized fractions in the $p/3$ series. Consider $\nu = p/3$. The prefactor in equation (50) increases by a factor p, while the effective box size also increases by the same factor. The net effect is that the expression for the gap is similar for all fractions $p/3$, where $p = 1, 2, 4, 5$, etc. Hence the energy gaps for the $p/3$ fractions measured across a range of samples should all fall on approximately the same curve as a function of magnetic field.

Equation (53) presented an analytic expression for $\tilde{\Delta}$ which, to the level of approximation employed, did not depend on the ground-state J_m-value. Examination of the more accurate versions of the hyperangular equation presented in section 2.3 suggests that $\tilde{\Delta}$ should actually have a weak but finite dependence on J_m (recall, for example, equation (23) or (24)). In the $N = 3$ study in section 2.2, we found that increasing J did indeed increase the localization of $G(\Omega')$ around the classical minima. For large N, as discussed in section 2.3, the dependence on J_m should be weaker; however, the resulting hybridization between a given SEM (i.e. WX) and nearest-neighbour SIMs (i.e. WXD) should also decrease slightly as J_m increases. Decreasing hybridization will reduce the value of $\tilde{\Delta}$ as J_m increases. It is interesting to analyse the effect of this reduction in $\tilde{\Delta}$ for the separate situations of (a) a given sample over a range of ν-values, and (b) different samples at a given fixed ν. In case (a), the number of electrons N is fixed. As the value of J_m increases, the value of ω_c at which this J_m-value represents the ground state must also increase. If $\tilde{\Delta}$ decreases as J_m increases, then $\tilde{\Delta}$ must also decrease with increasing ω_c. This reduction in $\tilde{\Delta}$ as ω_c increases, if sufficiently large, will make $\Delta E \to 0$; we suggest that this may be related to the predicted formation of a Wigner solid (i.e. gapless excitations) at very high magnetic fields. In case (b), fixed ν means that increasing J_m requires an increase in N (recall that $J_m = N(N-1)/(2\nu)$). If $\tilde{\Delta}$ decreases as J_m increases, then $\tilde{\Delta}$ must also decrease as N increases. However, a fixed value of ν means that increasing N requires an increase in magnetic field. Hence $\tilde{\Delta}$ decreases as ω_c increases. As mentioned earlier, this will tend to weaken the linear magnetic field dependence of the theoretical gaps at fixed ν to ω_c^x with $0 < x < 1$. Such a sub-linear dependence is consistent with recent experimental data at high fields [29]. In the estimates of the gap discussed below, however, we take as a first approximation the form of $\tilde{\Delta}$ presented in equation (53). Consequently the calculated gaps for a given ν always increase linearly with magnetic field.

We now proceed to discuss appropriate values of $\overline{[\delta a/a]}$, and hence calculate the gaps. The precise value for $\overline{[\delta a/a]}$ will depend on the details of the crystal plus defect system (WXD). Here we will suggest reasonable lower and upper estimates, and argue that the particular value to be used will depend on the degree of disorder in the experimental

samples. In particular, we will argue that the lower estimate is appropriate for disordered (i.e. lower-mobility) samples, while the upper estimate is appropriate for pure (i.e. higher-mobility) samples.

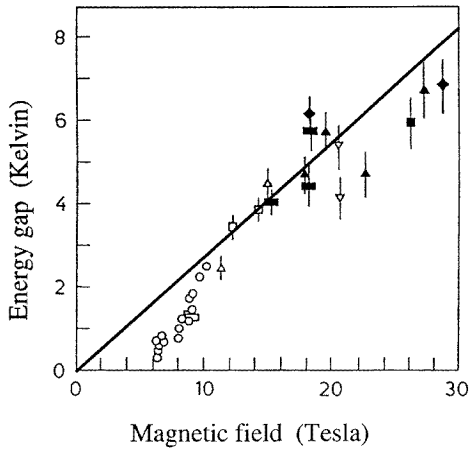

Figure 7. The theoretical lower estimate (straight line) for FQHE energy gaps obtained from the present theory as compared to experimental results over a range of lower-mobility GaAs heterostructure samples. (This figure was adapted from the data of Boebinger *et al*, references [27] and [3].) Experimental data: $\nu = \frac{1}{3}$ (black points), $\nu = \frac{2}{3}$ (white points). As discussed in the text, the theoretical gaps are the same for $\nu = \frac{1}{3}$ and $\nu = \frac{2}{3}$ to a first approximation.

First we consider the lower estimate for $\overline{[\delta a/a]}$. Fisher *et al* found that the maximum distortion for a vacancy defect was about 12%, but that the value for the interstitial defect was 'considerably larger' [26]. If the sample contains a significant impurity concentration, it is likely that interstitial electrons will have difficulty in diffusing through the N-electron system. The function $G(\Omega')$ will therefore have a restricted delocalization for kinetic reasons. In the absence of interstitial defects, the delocalization would be determined solely by the vacancies. We will therefore take the value of 12% as a lower estimated bound for $\overline{[\delta a/a]}$. From the appendix, we have that

$$\bar{e} \sim \frac{27\bar{h}^2 N^2}{16 m^* \pi^2}$$

and hence

$$\tilde{\Delta} \sim 0.4 \frac{\bar{h}^2 N^2}{m^* \pi^2}.$$

Substituting this into the expression for the energy gap, we obtain $\Delta E_{1/3} \sim 0.014 \bar{h}\omega_c$ meV and hence $\Delta E_{1/3} \sim 0.16 \bar{h}\omega_c$ K. Given that 1 meV $\equiv 1.728B$(T) (tesla) for GaAs, we obtain $\Delta E_{1/3} \sim 0.27B$(T) degrees Kelvin. Hence at $B = 20$ T, $\Delta E_{1/3} \sim 5.5$ K. Figure 7 compares this lower estimated bound of the energy gap at $\nu = \frac{1}{3}$ (and hence $\nu = \frac{2}{3}$, as explained above) with early experimental results obtained by Boebinger *et al* [27, 3] over a range of relatively impure samples (i.e. significant impurity concentration). The agreement is surprisingly good; however, we emphasize that our calculation is obviously fairly crude. Apart from improving the expression for $\Delta E_{1/3}$ given in equation (50), one could do a better job in calculating the localization energy $\tilde{\Delta}$ from equation (53). Such improvements would almost certainly render the calculation of energy gaps within the present model numerical,

although such calculations would be more straightforward than the original alternative of an N-electron diagonalization. Various numerical improvements will be presented in a future publication; the goal of the present paper is to pursue a purely analytical theory.

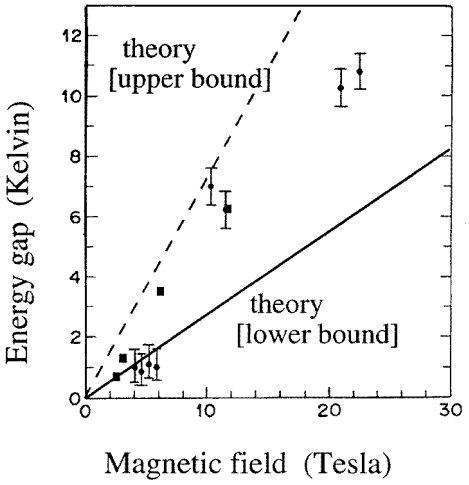

Figure 8. Theoretical upper (dashed line) and lower (solid line—the same as in figure 7) estimates for FQHE energy gaps obtained from the present theory as compared to experimental results over a range of higher-mobility GaAs heterostructure samples. The data were taken from reference [28] of Mallett *et al* (squares) and reference [30] of Willett *et al* (solid circles with error bars). The experimental data contain values for the fractions $\nu = p/3$, where $p = 1, 2, 4, 5$. As discussed in the text, the theoretical gaps are independent of p to a first approximation.

Now we turn to an upper estimate for $\overline{[\delta a/a]}$. We assume that the sample is pure, and hence that there is no kinetic reason for ignoring interstitial defects. We first recall our physical picture of the topology of the interstitial defect, stated earlier in this section. We consider a ring m containing N_m electrons, including particles $j-1$, j, and $j+1$ (cf. figure 5). The angle between particle j and $j+1$ is $2\pi/N_m$, and the angle between particle $j-1$ and $j+1$ is $4\pi/N_m$. We let the defect lie in the ring between particles j and $j+1$. We are looking for an upper estimate on the value of $\overline{[\delta a/a]}$; hence we will assume that the only particle which moves to accommodate the extra electron is particle j. As before, the angle between $j-1$ and $j+1$ is still $4\pi/N_m$, but now there are *two* particles (j and the defect) within this angular range. In an equilibrium state (i.e. a SIM), the three angles between $j-1$ and j, j and the defect, and the defect and $j+1$ are all equal to $4\pi/(3N_m)$. The distortion of the effective box size for particle j will be determined by the angle between j and $j+1$. Hence an estimate of the average distortion $\overline{[\delta a/a]}$ is $(2\pi/N_m)(\frac{4}{3}-1)$ divided by $2\pi/N_m$, which gives $\frac{1}{3}$. Our upper estimated value of $\overline{[\delta a/a]}$ is therefore 0.33. Figure 8 compares both this upper bound and the lower bound obtained earlier to experimental data obtained by the Oxford and AT&T groups for a range of relatively pure, high-mobility samples [28, 30]. The experimental values lie between the two bounds. This consistency between the present theoretical results and experiment lends support to our interpretation of the effect of sample purity.

4. Conclusions

A microscopic theory describing a confined N-electron gas in two dimensions, subject to an external magnetic field, was presented. The number of electrons N and the strength of the electron–electron interaction can be arbitrarily large. For any value of the magnetic field B, the correlated N-electron states were shown to be determined by the solution to a universal effective problem: this problem resembles that of a fictitious particle moving in a multi-dimensional space, without a magnetic field, occupied by potential minima corresponding to the classical N-electron equilibrium configurations.

A possible connection with the fractional (FQHE) and integer (IQHE) quantum Hall effects was subsequently proposed. In particular, it was shown that low-energy minima can arise in the large-N limit at filling factors $\nu = p/(2n+1)$, where p and n are any positive integers. The energy gaps calculated analytically at $\nu = p/3$ were found to be consistent with experimental data as a function of magnetic field, over a range of samples. Various other known features of FQHE and IQHE states were found to emerge from the present theory.

While it is obviously extremely difficult to calculate many-particle energy gaps, etc, accurately using an analytic approach, we hope that the general qualitative trends and orders of magnitude provided by the model will be useful in the understanding of the fascinating but complex field of highly correlated N-electron systems. We also hope that the model may begin to shed some light on the connection between the two limits of few-electron correlated states in quantum dots, and the infinite two-dimensional electron gas.

Acknowledgments

This work was supported by EPSRC Grant No GR/K 15619 (UK) and by COLCIENCIAS Project No 1204-05-264-94 (Colombia). We thank Professor Robin Nicholas and Dr V N Nicopoulos for useful comments toward the later stages of this work, and Dr P A Maksym for an earlier discussion. NFJ also thanks Professor P M Hui for discussing his unpublished results on few-electron classical configurations during a joint collaboration financed by the British Council under the UK–Hong Kong Joint Research Scheme.

Appendix

First we derive an approximate expression for $\bar{e}$ and hence $\tilde{\Delta}$. The exact hyperangular identity $\sum_{j=2}^{N}[X_j/r]^2 = 1$ implies that $\sum \alpha_j^2 \sim 1$. The moment of inertia I of the $(N-1)$-particle system in Ω space, treated as a rigid body, is therefore approximately just m^*. For large N, the density of particles will be approximately uniform: the moment of inertia for such a uniform disk is just $\frac{1}{2}(N-1)m^*R^2 \sim \frac{1}{2}Nm^*R^2$, where R represents the disk radius, and $(N-1)m^*$ is the total mass. Hence $R^2 \sim 2/N$, the average density of particles is $(N-1)/\pi R^2 \sim N^2/2\pi$, and the average particle–particle spacing is $\sim [2\pi]^{1/2}/N$. Now consider the sum over energies $e_j^{(J)}$ from equation (51):

$$\sum e_j^{(J)} \sim \sum \frac{\hbar^2\pi^2[N_m]^2}{2m^*\alpha_{j0}^2[4\pi]^2}. \tag{A1}$$

The quantity α_{j0} for particle j in ring m is approximately m times the average particle–particle separation: i.e. $\alpha_{j0} \sim m[2\pi]^{1/2}/N$. Replacing the sum over j by a sum over the

rings m, and using the approximate result that there are $6m$ particles in ring m, yields

$$\sum_j e_j^{(J)} \sim \sum_m [6m]^3 \frac{\bar{h}^2 N^2}{64 m^* \pi m^2} \sim \frac{27\bar{h}^2 N^2}{8 m^* \pi} \sum_1^{m_{max}} m \tag{A2}$$

where m_{max} is the maximum ring number. m_{max} is given approximately by the disk radius R divided by the particle–particle separation. Hence $m_{max}^2 \sim N/\pi$. For large m_{max}, $\sum_1^{m_{max}} m \sim \frac{1}{2} m_{max}^2$. Hence

$$\sum e_j^{(J)} \sim \frac{27\bar{h}^2 N^3}{16 m^* \pi^2}. \tag{A3}$$

We require the average $e_j^{(J)}$-value, $\bar{e}$, with the average taken over all j. There are $N-2$ such j-coordinates, and hence for large N we have

$$\bar{e} \sim \frac{27\bar{h}^2 N^2}{16 m^* \pi^2}$$

as claimed in section 4. Given that

$$\tilde{\Delta} \sim 2\overline{\left[\frac{\delta a}{a}\right]}\bar{e} \tag{A4}$$

we obtain

$$\tilde{\Delta} \sim \overline{\left[\frac{\delta a}{a}\right]} \frac{27\bar{h}^2 N^2}{8 m^* \pi^2} \tag{A5}$$

and hence $\tilde{\Delta} \sim N^2$ as claimed.

Second, we investigate the general N-dependence of E_0. Following equations (47) and (48), we assume that E_0 is dominated by the classical potential energy at the SEM $\Omega' \equiv \Omega_0'$, i.e. $E_0 \sim \beta V(\Omega_0')$. This is consistent with our assumption throughout the paper of considering configurations close to the classical minima. Hence

$$E_0 \sim \beta \sum_{j<j'} \frac{1}{|\alpha_{j0} e^{i\theta_{j0}} - \alpha_{j'0} e^{i\theta_{j'0}}|^2}. \tag{A6}$$

Replacing the denominator by $\overline{\alpha^2}$ yields

$$E_0 \sim \beta \frac{1}{\overline{\alpha^2}} \sum_{j<j'} 1$$

and hence $E_0 \sim \beta N \frac{1}{2}(N-1)(N-2)$. For large N, $E_0 \sim \beta N^3/2$, and hence $E_0 \sim N^3$ as claimed. We note that while this derivation is crude, the final expression for E_0 is not actually used in the calculation of the energy gaps. The only result used is the conclusion that $E_0 \gg \tilde{\Delta}$ for large N.

References

[1] Prange R E and Girvin S M 1990 *The Quantum Hall Effect* (New York: Springer)
[2] MacDonald A H 1990 *Quantum Hall Effect: a Perspective* (New York: Academic)
[3] Chakraborty T and Pietilainen P 1995 *The Quantum Hall Effects* (Heidelberg: Springer)
[4] Laughlin R B 1983 *Phys. Rev. Lett.* **50** 1395
[5] Halperin B I 1983 *Helv. Phys. Acta* **56** 75
Halperin B I 1986 *Sci. Am.* **254** 52
[6] Jain J K 1993 *Adv. Phys.* **41** 105
[7] Halperin B I, Lee P A and Read N 1993 *Phys. Rev.* B **47** 7312

[8] Ashoori R C, Stormer H L, Weiner J S, Pfeiffer L N, Baldwin K W and West K W 1993 *Phys. Rev. Lett.* **71** 613
[9] McEuen P L, Foxman E B, Kinaret J, Meirav U, Kastner M A, Wingreen N S and Wind S J 1992 *Phys. Rev.* B **45** 11 419
[10] Maksym P A and Chakraborty T 1990 *Phys. Rev. Lett.* **65** 108
Hawrylak P 1993 *Phys. Rev. Lett.* **71** 3347
Yang S-R E, MacDonald A H and Johnson M D 1993 *Phys. Rev. Lett.* **71** 3194
Hawrylak P and Pfannkuche D 1993 *Phys. Rev. Lett.* **70** 485
[11] See, for example,
Hansen W, Smith T P, Lee K Y, Hong J M and Knoedler C M 1990 *Appl. Phys. Lett.* **56** 168
[12] Johnson N F and Quiroga L 1995 *Phys. Rev. Lett.* **74** 4277
[13] Bolton F and Rossler U 1993 *Superlatt. Microstruct.* **13** 140
[14] Bedanov V M and Peeters F M 1994 *Phys. Rev.* B **49** 2667
[15] Maksym P A 1996 *Phys. Rev.* B **53** 10 871
Some related ideas were presented by
Hausler W and Kramer B 1993 *Phys. Rev.* B **47** 16 353
See also
Maksym P A 1997 *Proc. 1996 High Magnetic Field Conf. (Wurzburg)* (Singapore: World Scientific)
[16] Kivelson S, Kallin C, Arovas D P and Schrieffer J R 1986 *Phys. Rev. Lett.* **56** 873
Kivelson S, Kallin C, Arovas D P and Schrieffer J R 1987 *Phys. Rev.* B **36** 1620
[17] Johnson N F 1995 *J. Phys.: Condens. Matter* **7** 965
Quiroga L, Ardila D and Johnson N F 1993 *Solid State Commun.* **86** 775
[18] Hallam L D, Weis J and Maksym P A 1996 *Phys. Rev.* B **53** 1452
[19] Madhav A V and Chakraborty T 1994 *Phys. Rev.* B **49** 8163
[20] Kinaret J M, Meir Y, Wingreen N S, Lee P and Wen X-G 1992 *Phys. Rev.* B **46** 4681
[21] Hui P M 1996 unpublished
[22] This terminology follows that introduced in molecular physics and later adopted by Maksym in reference [15]. See
Wilson E B 1935 *J. Chem. Phys.* **3** 276
[23] Fock V 1926 *Z. Phys.* **47** 446
[24] Geller M R and Vignale G 1996 *Phys. Rev.* B **53** 6979
[25] Schweigert V A and Peeters F M 1995 *Phys. Rev.* B **51** 7700
[26] Fisher D S, Halperin B I and Morf R 1979 *Phys. Rev.* B **20** 4692
[27] Boebinger G S, Stormer H L, Tsui D C, Chang A M, Hwang J C M, Cho A Y, Tu C W and Weimann G 1987 *Phys. Rev.* B **36** 7919
[28] Mallett J R, Clark R G, Nicholas R J, Willett R, Harris J J and Foxon C T 1988 *Phys. Rev.* B **38** 2200
[29] Leadley D R, van der Burgt M, Nicholas R J, Foxon C T and Harris J J 1996 *Phys. Rev.* B **53** 2057
[30] Willett R L, Stormer H L, Tsui D C, Gossard A C and English J H 1988 *Phys. Rev.* B **37** 8476